NASA
Technical
Paper
2206

September 1983

Aerodynamic Characteristics of a Series of Bodies With Variations in Nose Camber

Barrett L. Shrout
and Peter F. Covell

NASA

25th Anniversary
1958-1983

NASA
Technical
Paper
2206

1983

Aerodynamic Characteristics of a Series of Bodies With Variations in Nose Camber

Barrett L. Shrout
and Peter F. Covell

Langley Research Center
Hampton, Virginia

NASA
National Aeronautics
and Space Administration

Scientific and Technical
Information Branch

SUMMARY

An investigation of the aerodynamic characteristics of a series of cambered forebody models having a systematic variation in nose droop angle was conducted in the Langley 8-Foot Transonic Pressure Tunnel at Mach numbers from 0.60 to 1.20 and in the Langley Unitary Plan Wind Tunnel at Mach numbers of 1.47, 1.80, and 2.16. The forebodies had a fineness ratio of 3 and were attached through a transition section to a cylindrical afterbody. The models were tested through an angle-of-attack range of about 0° to 12° in the 8-Foot Transonic Pressure Tunnel and -2° to 20° in the Unitary Plan Wind Tunnel. Static longitudinal aerodynamic characteristics of the models were determined for all Mach numbers, and lateral-directional characteristics were determined for Mach numbers of 1.47 to 2.16.

The investigation indicated that the principal effect of varying nose droop was on pitching moment, with some secondary effects on lift and drag. All the models exhibited the characteristic aerodynamic behavior of forebody/cylindrical afterbody configurations; that is, most of the lift at low angles of attack was apparently generated on the forebody, while for higher angles of attack, the data implied considerable afterbody lift generated by separated cross-flow drag. Two computer methods were used to predict wave drag. The results were compared with experimental data for supersonic Mach numbers.

INTRODUCTION

Modern high-speed aircraft, especially those used by the military services, frequently require a large amount of over-the-nose visibility, in particular during the approach and landing phase of flight. Although canopy height is an obvious factor in determining visibility over the nose, increased canopy height is often accompanied by increased drag, which could be especially significant for aircraft with a supersonic performance requirement. Over-the-nose visibility can also be increased by drooping the nose, which may have the additional advantage of reducing the length of the nose gear.

Some previous studies of nose droop and forebody camber are reported in references 1 through 5. Generally, these studies consisted of wind-tunnel tests of body shapes with a relatively small range of nose droop, or wing-body-tail arrangements with various amounts of forebody camber. As might be expected, the most significant effects were noted in pitching moment and lift, with some changes in drag. The general characteristics of the flow over a forebody with a cylindrical or near-cylindrical afterbody have been discussed in references 6 and 7 and, more recently, in reference 8. At low angles of attack, virtually all the lift is inviscid lift generated on the forebody. At higher angles of attack, however, viscous cross flow over the afterbody separates, which results in a substantial contribution to the normal force.

The present investigation was initiated to determine the aerodynamic effects associated with a systematic variation of nose droop angle for a body with a circular cross section. The baseline configuration from which the drooped-nose models were derived had a forebody with a fineness ratio of 3 and a cylindrical afterbody. A series of six models were constructed with nose droop angles varying from 0° to -20° in 4° increments. These models were tested in the Langley 8-Foot Transonic Pressure

Tunnel at Mach numbers from 0.60 to 1.20 at a Reynolds number of 3.2×10^6 per foot (10.5×10^6 per meter), and in the Langley Unitary Plan Wind Tunnel at Mach numbers of 1.47, 1.80, and 2.16 at a Reynolds number of 2.0×10^6 per foot (6.6×10^6 per meter). Estimates were made of the wave drag of the various models at supersonic Mach numbers by using both a near-field method and a far-field method. The results of the experimental and theoretical investigations are presented herein.

SYMBOLS

Force and moment data are referenced to the body axis system except for lift and drag data, which are referenced to the stability axis system. The moment reference center for the model is located at 9.0 in. (23 cm) from the model nose apex and on the horizontal reference line.

The data are presented in U.S. Customary Units with SI Units in parentheses. The symbols are defined as follows:

A	cross-sectional area, in^2 (cm^2)
b	base diameter, 2.00 in. (5.08 cm)
C_D	drag coefficient, Drag/qS
$C_{D,c}$	base cavity drag coefficient, Base cavity drag/qS
$C_{D,o}$	drag coefficient at $C_L = 0$
$C_{D,w}$	wave drag coefficient
C_L	lift coefficient, Lift/qS
$C_{L,o}$	lift coefficient at $\alpha = 0$
C_{L_α}	lift-curve slope at $C_L = 0$, per degree
C_l	rolling-moment coefficient, Rolling moment/qSb
C_{l_β}	roll-stability parameter, per degree
C_m	pitching-moment coefficient, Pitching moment/qS$\bar{c}$
$C_{m,o}$	pitching-moment coefficient at $C_L = 0$
$\partial C_m/\partial C_L$	longitudinal stability parameter at $C_L = 0$
C_n	yawing-moment coefficient, Yawing moment/qSb
C_{n_β}	directional stability parameter, per degree
C_Y	side-force coefficient, Side force/qS
C_{Y_β}	side-force parameter, per degree

$\bar{c}$ reference length, base diameter, 2.00 in. (5.08 cm)

L/D lift-drag ratio

l overall length of model, 19.0 in. (48.3 cm)

M free-stream Mach number

q free-stream dynamic pressure, psf (Pa)

r body radius, in. (cm)

S reference area, base area, 3.142 in^2 (20.27 cm^2)

x longitudinal distance from nose of model, in. (cm)

z_c vertical distance of mean line from horizontal reference line, in. (cm)

α angle of attack, deg

β angle of sideslip, deg

θ angle of nose droop, deg, positive up

Subscript:

max maximum

Abbreviation:

Conf. configuration

DESCRIPTION OF MODELS

Sketches of the profiles of the six models used in this investigation are shown in figure 1, and a photograph of the models is shown in figure 2. Each model consists of a forebody with a fineness ratio of 3, a transition section with constant cross-sectional area, and a common cylindrical afterbody. The longitudinal area distribution of the forebodies is identical to that of a tangent ogive of the same length and fineness ratio. The model geometry of each of the forebodies was developed by shearing the circular cross sections of the tangent ogive vertically so that the upper surface at the plane of symmetry was a straight line inclined at an angle θ, defined as the angle of nose droop. The angle was varied from 0° for configuration 1 to -20° for configuration 6 in increments of 4°. For each model, a transition section was designed which was tangent to the forebody at its base and tangent to the cylindrical afterbody. Some of the geometric characteristics of the models including the radius and mean line variations along the x-axis are given in table I, and a plot of the normal area distribution, which was identical for all models, is shown in figure 3.

TEST CONDITIONS, INSTRUMENTATION, AND DATA CORRECTIONS

Wind-tunnel tests at subsonic and transonic Mach numbers ($M \leq 1.2$) were conducted in the Langley 8-Foot Transonic Pressure Tunnel, and tests at supersonic Mach numbers were conducted in the Langley Unitary Plan Wind Tunnel.

The subsonic-transonic tests were conducted at a Reynolds number of 3.2×10^6 per foot (10.5×10^6 per meter), and boundary layer transition was fixed on the model by means of a 0.10-in. (0.25-cm) wide strip of No. 120 carborundum grit, located 1.5 in. (3.8 cm) aft of the model nose apex.

The supersonic tests were conducted at a Reynolds number of 2.0×10^6 per foot (6.6×10^6 per meter), and the boundary layer transition strip consisted of a 0.063-in. (0.159-cm) wide band of No. 50 carborundum grit located 1.2 in. (3.0 cm) aft of the model nose apex.

Some of the other test conditions are shown in the following chart:

M	Stagnation pressure		Stagnation temperature	
	psf	kPa	°F	K
0.60	2137	102.3	120	322
.80	1796	86.0	120	322
.90	1705	81.6	120	322
.95	1673	80.1	120	322
1.10	1617	77.4	120	322
1.20	1606	76.9	120	322
1.47	1103	52.8	150	339
1.80	1220	58.4	150	339
2.16	1430	68.3	150	339

Forces and moments were measured by means of a six-component strain-gage balance contained within the model. The balance was attached through a supporting sting to the permanent model-actuating systems in the wind tunnels. Base cavity pressures were measured by means of two tubes routed along the sting and to the outside of the tunnel, where they were connected to two pressure transducers. These pressures were measured throughout the test program in order to correct the data to a condition of free-stream static pressure acting over the total model base.

The base drag variations are shown in figure 4. In general, the base drag increased as angle of attack increased above values of about 4°. At constant angle of attack, the base drag became greater with increasing Mach number up to 1.10. Above $M = 1.20$, the base drag decreased with increasing Mach number. Larger than average variations in base drag between models at Mach numbers 1.10 and of 1.20 were most likely caused by the reflected bow shock impacting the sting near the model base.

The data were corrected for deflections of the balance-sting combination due to aerodynamic loads. The data for $M = 1.47$ and above were corrected for test section flow angularity.

RESULTS AND DISCUSSION

Experimental Data

Some of the static longitudinal aerodynamic characteristics of the six models of this investigation are presented in figure 5. At Mach numbers below 1.00, the most noticeable effect of increasing nose droop is a sizeable reduction in pitching moment. The pitching-moment increment due to nose-droop-angle variation remains nearly constant up to a lift coefficient of about 0.5. The lift-curve slopes are reasonably linear near zero lift and increase with increasing angle of attack by amounts which are an inverse function of the nose droop angle. The low values of lift-curve slope and the instability of the pitching-moment curves imply that most of the lift is generated on the forebody. The drag variation with lift is essentially parabolic, while the lift coefficient for minimum drag tends to increase slightly as nose droop is increased. There are only minor differences in the lift-drag ratio (L/D) for the various models at subsonic Mach numbers.

At Mach numbers of 1.10 and 1.20, the lift and pitching-moment characteristics are similar to the data for Mach numbers less than 1.00; however, the increased separation between the drag polars is probably the result of the effect of nose droop on wave drag. The differences in the drag polars occur at relatively low values of lift so that the L/D variations for the different models fall in a narrow band.

For Mach numbers of 1.47 and above, data were taken at angles of attack up to about 20°. The data at low angles of attack are similar to the subsonic data; that is, generally low values of lift-curve slope and unstable pitching-moment variations for the reference moment center. At higher angles of attack, the increasing lift-curve slopes and reduced instability of the pitching-moment curves imply increased lift on the afterbody due to separated cross flow. These characteristics are typical of forebody-afterbody configurations as discussed in references 6 through 8. For model 1 and, to a lesser extent, for models 2 and 3, the forebody apparently also develops some separated cross flow, since more lift is produced at a given angle of attack, and the less stable pitching-moment variation indicates that the center of lift is closer to the model apex. The differences in flow behavior for the various models tend to decrease with increasing Mach number so that for $M = 2.16$, the lift variation with angle of attack and the pitching-moment variation with lift coefficient are similar for all the models.

The substantial loss of lift at low angles of attack for the models with the highest degree of nose droop indicates the possibility of some cross-flow separation on the lower surface of those models. Although the models with the least amount of nose droop have lower minimum drag, higher levels of drag-due-to-lift result in lower values of maximum L/D than for the models with greater nose droop. The maximum value of lift-drag ratio at supersonic speeds is on the order of 2.3.

Figure 6 shows the variation of some of the longitudinal aerodynamic parameters with Mach number. The increment in $C_{m,o}$ for the various models remains relatively constant over the Mach number range. Models 1 and 2 have positive $C_{m,o}$, while the other models all have negative $C_{m,o}$. The variation of $C_{m,o}$ with Mach number is reasonably linear except for a dip around $M = 1.10$.

For Mach numbers less than 1.00, there is a maximum variation of about 25 percent in $C_{D,o}$ between models 1 and 6, while at supersonic Mach numbers, the maximum variation is about 35 percent. Levels of $C_{D,o}$ for any particular Mach number are approximately equal for models 1, 2, and 3, and become increasingly greater for models 4, 5, and 6 at supersonic speeds.

The variation of C_L at $\alpha = 0$ with nose droop angle is due to camber or effective angle of attack, although the slightly negative values of $C_{L,o}$ for models 1 and 2 at the lower Mach numbers were not expected. The differences in $C_{L,o}$ between the various models in general increase with increasing Mach numbers.

The longitudinal stability parameter is measured near $C_L = 0$ and, with the exception of model 6, is relatively constant for Mach numbers above 1.40 and for Mach numbers less than 0.90. Model 6 is less unstable at high and low Mach numbers and more unstable at the intermediate Mach numbers than any of the other models.

The lift-curve slope, measured near $C_L = 0$, generally increased slightly with increasing Mach number for models 1, 2, and 3. For models 4, 5, and 6, the levels of C_{L_α} increased with increasing nose droop but did not vary in a consistent manner with changes in Mach numbers.

Static lateral and directional data are presented in figures 7 through 9. The model-sting installations were dynamically unstable during the tests in the 8-Foot Transonic Pressure Tunnel. The instability became more critical when the models were yawed. As a consequence, sideslip data were obtained in this tunnel only for model 6. Figure 7 shows coefficients of yawing moment, rolling moment, and side force versus angle of attack for sideslip angles of 0° and 5° at Mach numbers up to 1.20. Yawing the model generated a substantial rolling moment, which was essentially unaffected by changes in either angle of attack or Mach number. The substantial side-force increment caused by yaw tended to increase at angles of attack above 4° and also as Mach number increased. Yawing the model apparently caused afterbody separation at a lower angle of attack, with a resultant change in direction of the yawing moment. The angle of attack at which this change in direction occurred decreased with increasing Mach number through $M = 1.10$.

Figure 8 presents coefficients of yawing moment, rolling moment, and side force for models 2, 4, and 6 at three angles of attack over a range of sideslip angles for Mach numbers of 1.47 and 2.16. Because the variation of the coefficients is reasonably linear for sideslip angles between 4° and -4°, lateral-directional stability derivatives were calculated for all the models and are presented in figure 9. These stability derivatives were calculated from data taken at angles of sideslip of 0° and 3°. The roll-stability parameter increases in a near-linear fashion with increasing nose droop angle and varies little with changes in angle of attack or Mach number, with the exception of model 6, which produces a decrease in rolling-moment derivative with increasing angle of attack.

All the models are directionally unstable at low angles of attack, and the models with small nose droop angles remain unstable at the higher angles of attack, where the afterbody forces predominate. The models with large nose droop angles become directionally stable at the higher angles of attack. This directional stability becomes of considerable significance as the supersonic flight regimes of fighter aircraft and missiles are expanded to higher angles of attack. All models exhibited side-force stability which increased by varying amounts as angle of attack was increased.

For this investigation, the angle-of-attack range below 8° or 10° provides the most significant data for application of a drooped nose to a conventional aircraft configuration. For higher angles of attack, the data are strongly influenced by the viscous cross flow over the cylindrical afterbody, which may not be representative of an aircraft fuselage.

Comparison of Experiment and Theory

The wave drag of the six models at supersonic Mach numbers was computed by two methods described in references 9 and 10. The method of reference 9, a far-field wave drag method, is based on slender body theory and the supersonic area rule. The zero-lift wave drag of a configuration is determined by taking a weighted average of the wave drags for several equivalent bodies of revolution formed by passing a series of Mach planes through the configuration at various azimuth angles.

The method of reference 10 is a near-field method and uses a modified linear-theory with exact boundary conditions and local Mach number corrections to calculate pressure distributions over the configuration surface. These pressure distributions are integrated for lift, drag, and pitching moment. This method is not limited to the zero-lift drag condition and can be used to calculate pressure distributions and forces and moments for various angles of attack.

Both methods were used to compute the wave drag of the six models for Mach numbers of 1.20, 1.47, 1.80, and 2.16. The geometry of the models was input into the two programs in the $\alpha = 0°$ orientation. It should be noted that this, in general, is not the orientation for zero lift, as can be seen from the data in figure 5.

Experimental values of wave drag coefficient were determined by subtracting skin-friction drag coefficients, calculated by the method of reference 11, from the experimental drag coefficients for $\alpha = 0°$. The experimental data and theoretical estimates are shown in figure 10 as a function of nose droop angle for various supersonic Mach numbers.

The far-field wave drag program predicts the trends, if not the absolute drag levels, for Mach numbers of 1.20 and 1.47. At the higher Mach numbers, there are substantial differences between theory and experiment, particularly for models 1 and 6, which have the most extreme camber. The effect of this camber coupled with the higher Mach numbers is that the program interprets the configuration geometry to be an extremely blunt body for certain Mach plane orientations. The blunt body interpretation severely violates the slender body assumption of the theoretical method and results in gross overprediction of the wave drag. It would appear that for Mach numbers above 1.80, anything more than a few degrees of camber will cause errors in the far-field drag prediction. It should be noted that for a complete configuration, the forebody contribution will be somewhat masked in the overall wave drag.

With the exception of model 1 ($\theta = 0°$), the modified linear theory method of reference 10 predicts the trends of wave drag coefficient versus nose droop angle for Mach numbers 1.47 through 2.16, although the levels are slightly low for Mach numbers 1.80 and 2.16. The level of the wave drag coefficient and its variation with nose droop angle are not well predicted for a Mach number of 1.20.

CONCLUDING REMARKS

A series of forebody models having various degrees of nose droop have been tested in a wind-tunnel investigation at Mach numbers from 0.60 to 2.16. The forebodies were attached to a cylindrical afterbody. The results of this investigation are summarized below.

All the models exhibited the characteristic aerodynamic behavior of forebody/cylindrical afterbody configurations; that is, most of the lift at low angles of attack was apparently generated on the forebody, while for higher angles of attack, the data implied considerable afterbody lift generated by separated cross-flow drag. As the nose droop angle was increased, a decrease in lift at constant angle of attack and a decrease in zero-lift pitching moment were measured. Minimum drag also increased, but reduced drag-due-to-lift resulted in higher lift-drag ratios for the models with higher droop angles, especially at supersonic speeds.

At supersonic speeds, the roll-stability parameter was relatively constant with changes in angle of attack, and its magnitude was essentially proportional to the amount of nose droop. All the models were directionally unstable at small angles of attack, but at larger angles of attack, the models with greater nose droop became directionally stable.

Of the two methods used to predict the zero-lift wave drag of the drooped nose models, a far-field method worked reasonably well for Mach numbers of 1.20 and 1.47, while a near-field method worked reasonably well for Mach numbers of 1.47, 1.80, and 2.16.

Langley Research Center
National Aeronautics and Space Administration
Hampton, VA 23665
August 10, 1983

REFERENCES

1. Spencer, Bernard, Jr.; Phillips, W. Pelham; and Fournier, Roger H.: Supersonic Aerodynamic Characteristics of a Series of Bodies Having Variations in Fineness Ratio and Cross-Section Ellipticity. NASA TN D-2389, 1964.

2. Gapcynski, John P.: The Effect of Camber on the Aerodynamic Characteristics of a Body at a Mach Number of 2.01. NASA TM X-56, 1959.

3. Dickey, Robert R.: Effect of Camber on the Drag of a Body of Revolution. NACA RM A56E23, 1956.

4. Boyd, John W.; and Menees, Gene P.: Longitudinal Stability and Control Characteristics at Mach Numbers From 0.70 to 2.22 of a Triangular Wing Configuration Equipped With a Canard Control, a Trailing-Edge-Flap Control, or a Cambered Forebody. NASA MEMO 4-21-59A, 1959.

5. Spearman, M. Leroy; and Driver, Cornelius: Effects of Forebody Deflection on the Stability and Control Characteristics of a Canard Airplane Configuration With a High Trapezoidal Wing at a Mach Number of 2.01. NASA MEMO 4-4-59L, 1959.

6. Allen, H. Julian; and Perkins, Edward W.: A Study of Effects of Viscosity on Flow Over Slender Inclined Bodies of Revolution. NACA Rep. 1048, 1951. (Supersedes NACA TN 2044.)

7. Chin, S. S.: Missile Configuration Design. McGraw-Hill Book Co., Inc., c.1961, pp. 18-29.

8. Barger, Raymond L.; and Sawyer, Wallace C.: Investigation of Flow Characteristics Over Missile Bodies at Supersonic Speeds. NASA TP-1579, 1979.

9. Harris, Roy V., Jr.: An Analysis and Correlation of Aircraft Wave Drag. NASA TM X-947, 1964.

10. Stancil, Robert T.: Improved Wave Drag Predictions Using Modified Linear Theory. J. Aircr., vol. 16, no. 1., Jan. 1979, pp. 41-46.

11. Sommer, Simon C.; and Short, Barbara J.: Free-Flight Measurements of Turbulent-Boundary-Layer Skin Friction in the Presence of Severe Aerodynamic Heating at Mach Numbers From 2.8 to 7.0. NACA TN 3391, 1955.

TABLE 1.- GEOMETRIC CHARACTERISTICS OF THE MODELS

x/l	r/r_{max}	Z_c/r_{max}					
		Conf. 1	Conf. 2	Conf. 3	Conf. 4	Conf. 5	Conf. 6
0.0000	0.0000	1.0000	0.4756	-0.0530	-0.5906	-1.1421	-1.7130
.0132	.0837	.9163	.4094	-.1016	-.6212	-1.1541	-1.7053
.0263	.1635	.8365	.3471	-.1463	-.6479	-1.1622	-1.6945
.0395	.2394	.7606	.2887	-.1870	-.6706	-1.1664	-1.6796
.0526	.3115	.6885	.2341	-.2240	-.6896	-1.1668	-1.6605
.0789	.4444	.5556	.1361	-.2866	-.7162	-1.1564	-1.6116
.1053	.5624	.4376	.0531	-.3344	-.7279	-1.1310	-1.5476
.1316	.6659	.3341	-.0154	-.3676	-.7251	-1.0911	-1.4691
.1579	.7560	.2449	-.0688	-.3856	-.7072	-1.0360	-1.3750
.1842	.8303	.1697	-.1099	-.3915	-.6773	-.9688	-1.2697
.2105	.8916	.1084	-.1363	-.3825	-.6320	-.8867	-1.1484
.2368	.9391	.0609	-.1488	-.3597	-.5733	-.7908	-1.0119
.2632	.9720	.0280	-.1488	-.3243	-.5019	-.6823	-.8670
.2895	.9932	.0068	-.1330	-.2733	-.4143	-.5582	-.7038
.3158	1.0000	.0000	-.1048	-.2098	-.3153	-.4216	-.5290
.3421	↓	↓	-.0724	-.1428	-.2185	-.2832	-.3540
.3684			-.0464	-.0913	-.1396	-.1804	-.2250
.3947			-.0263	-.0513	-.0785	-.1011	-.1260
.4211			-.0119	-.0228	-.0350	-.0448	-.0560
.4474			-.0033	-.0057	-.0090	-.0111	-.0140
.4737			.0000	.0000	.0000	.0000	.0000
1.0000			.0000	.0000	.0000	.0000	.0000

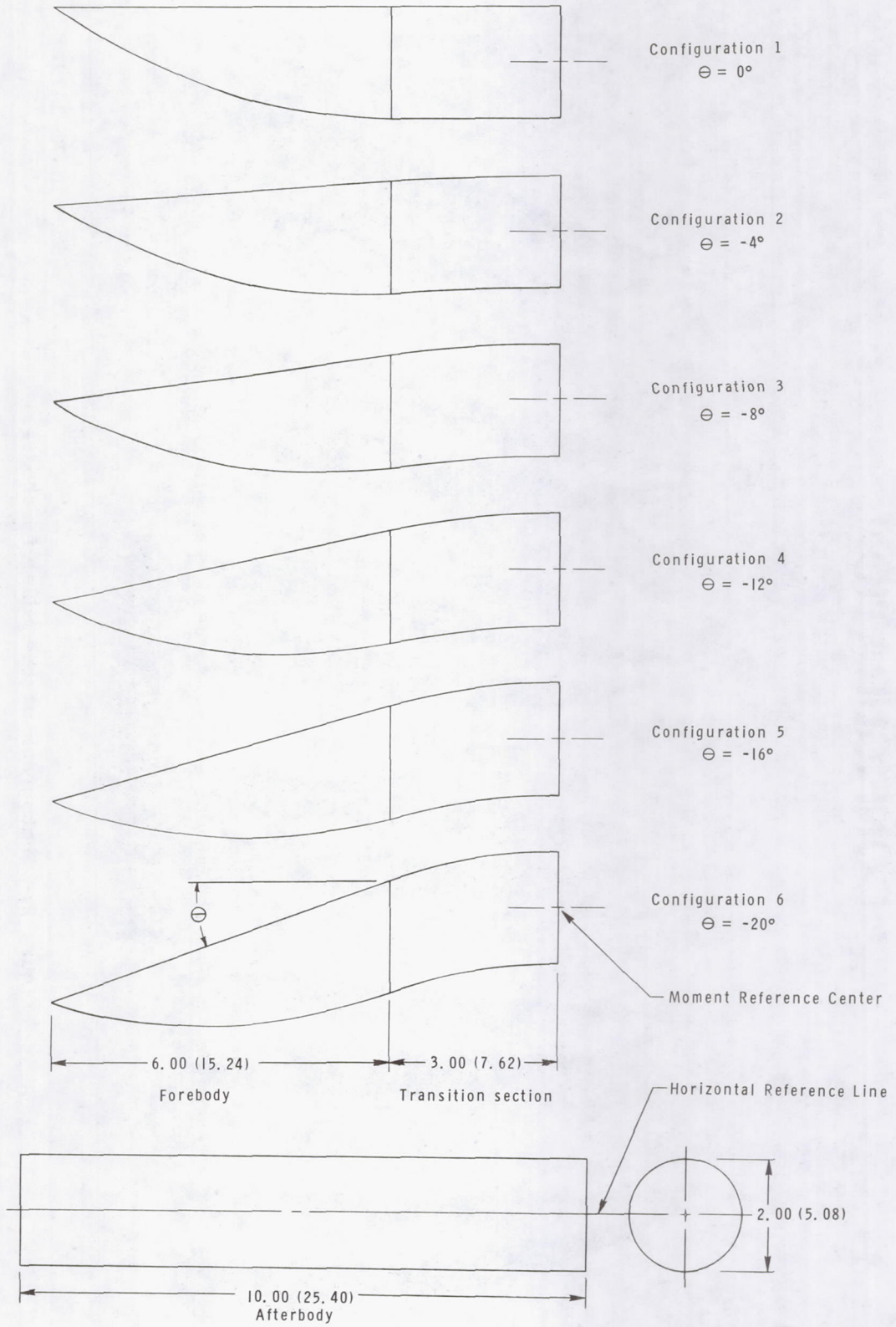

Figure 1.- Sketches of the models. All dimensions in inches (centimeters).

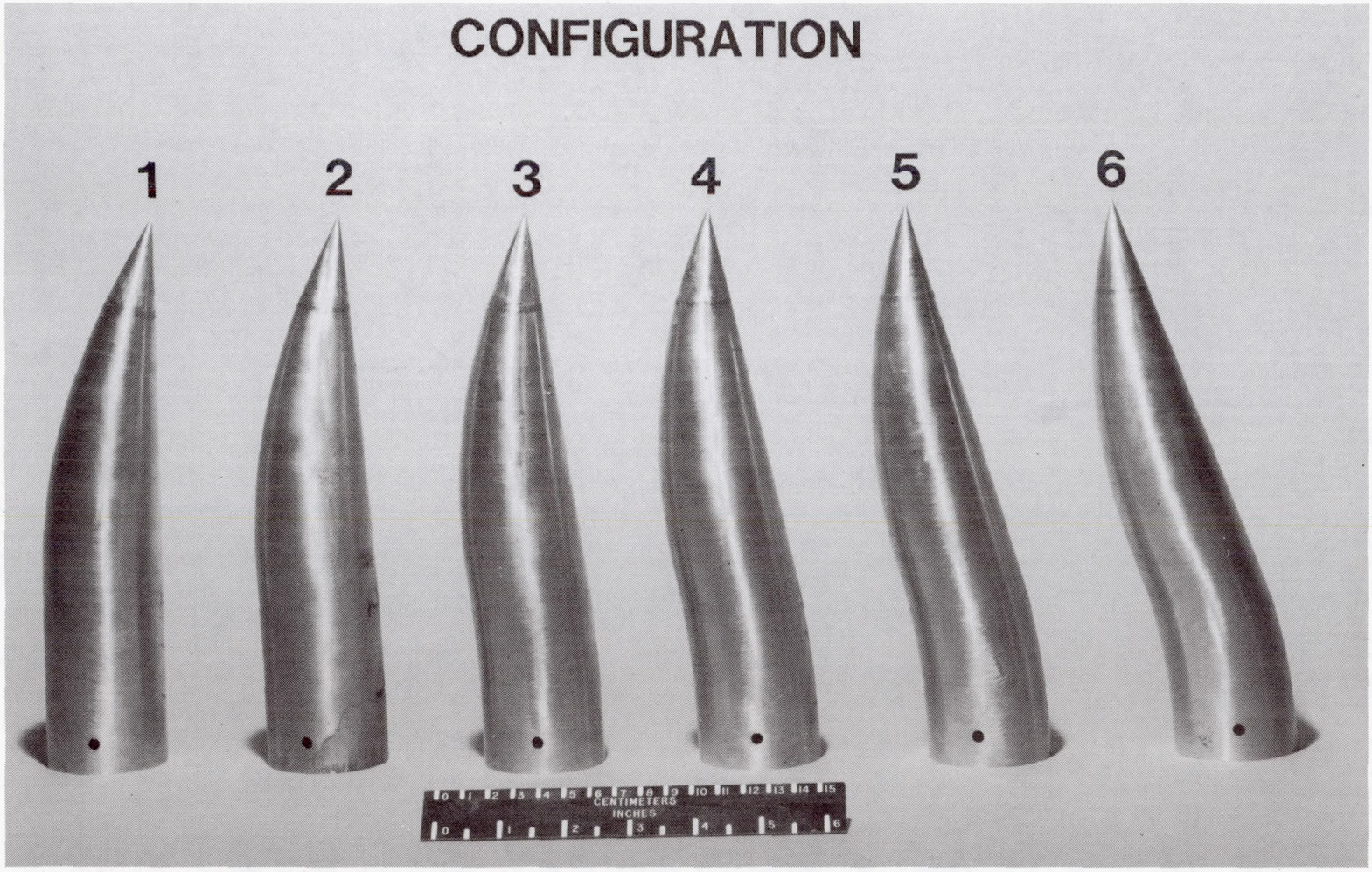

L-78-3472.1

Figure 2.- Photograph of the model forebodies.

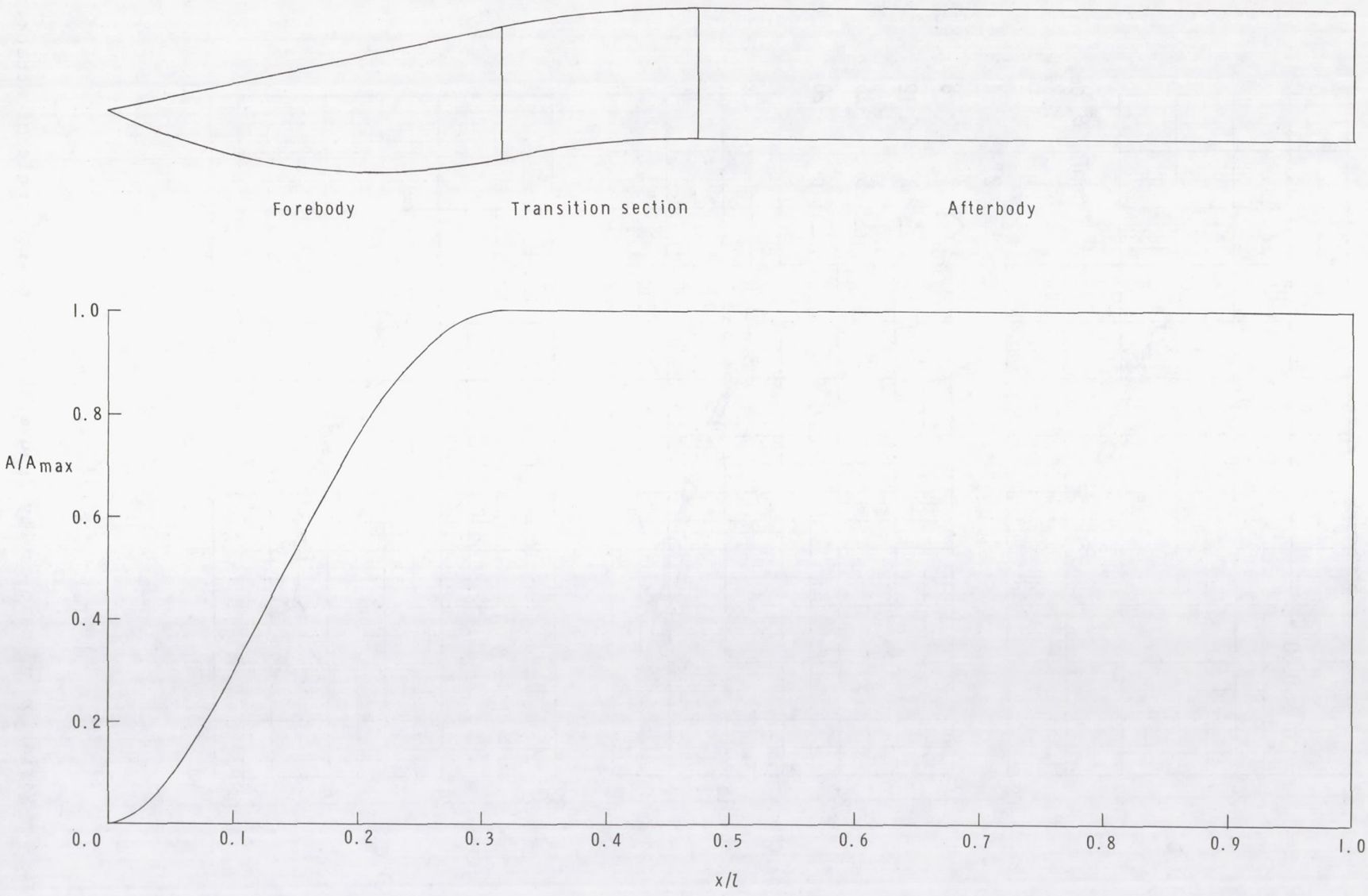

Figure 3.- Model normal area distribution.

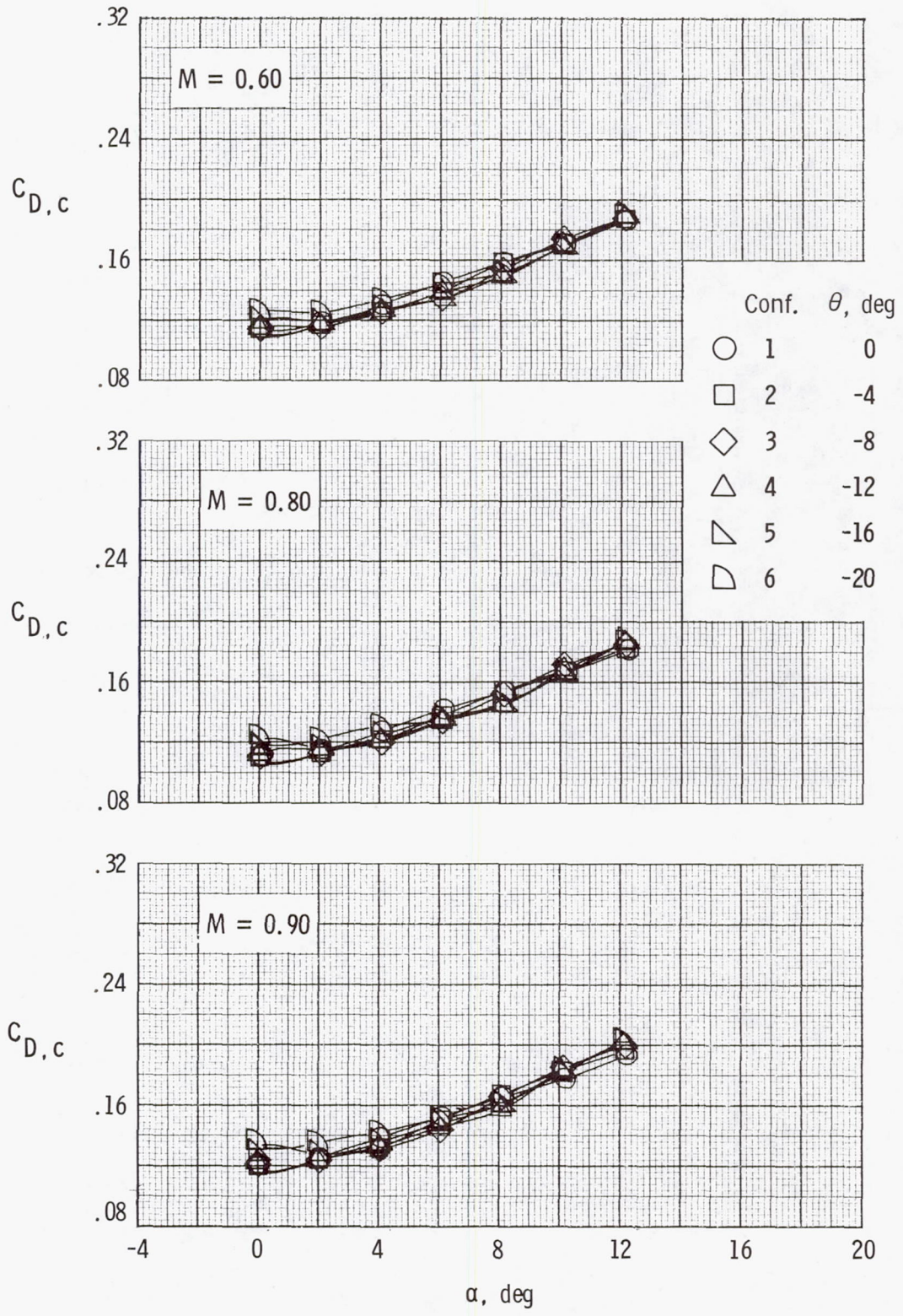

(a) M = 0.60 to 0.90.

Figure 4.- Variation of base cavity drag coefficient with angle of attack.

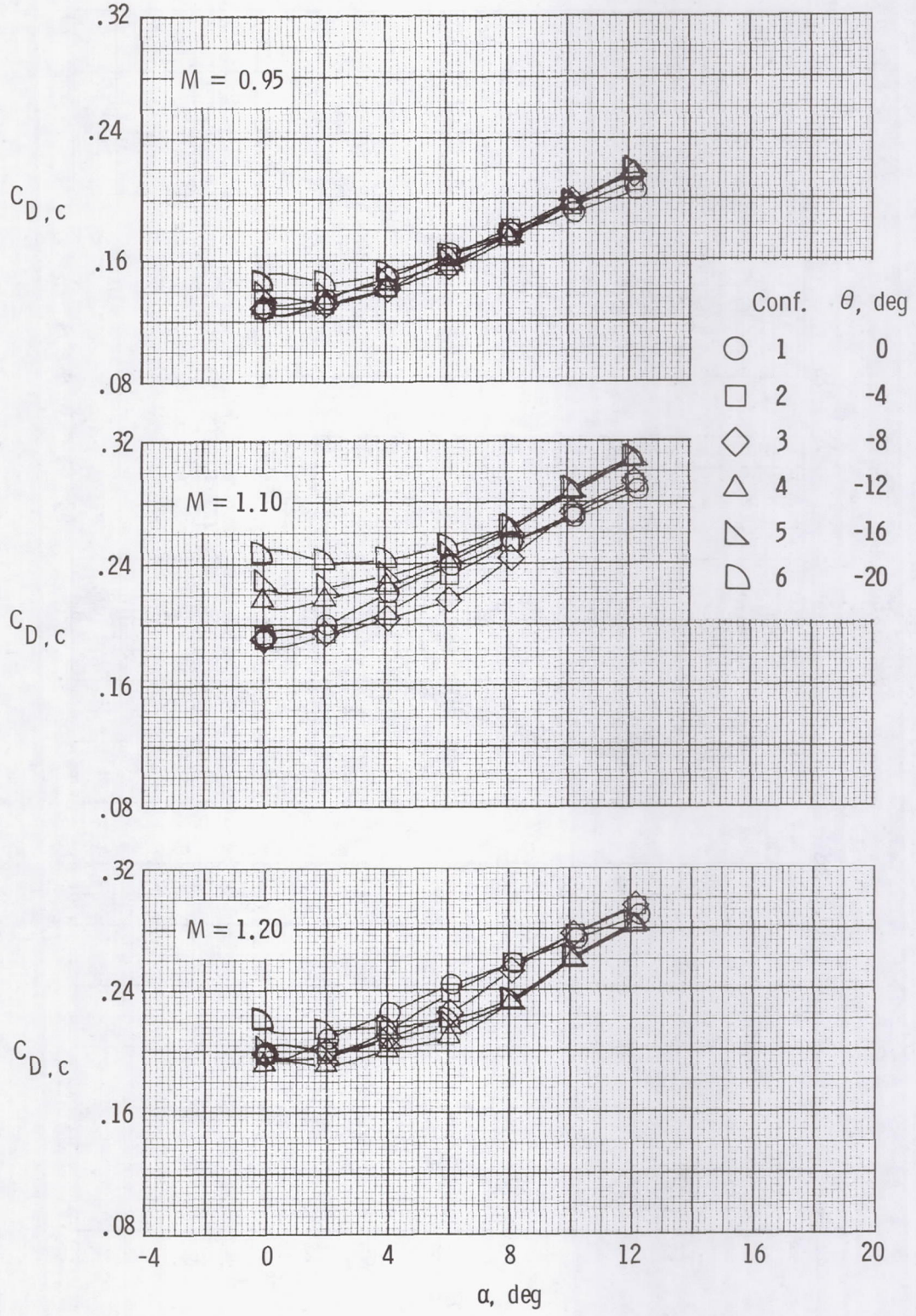

(b) M = 0.95 to 1.20.

Figure 4.- Continued.

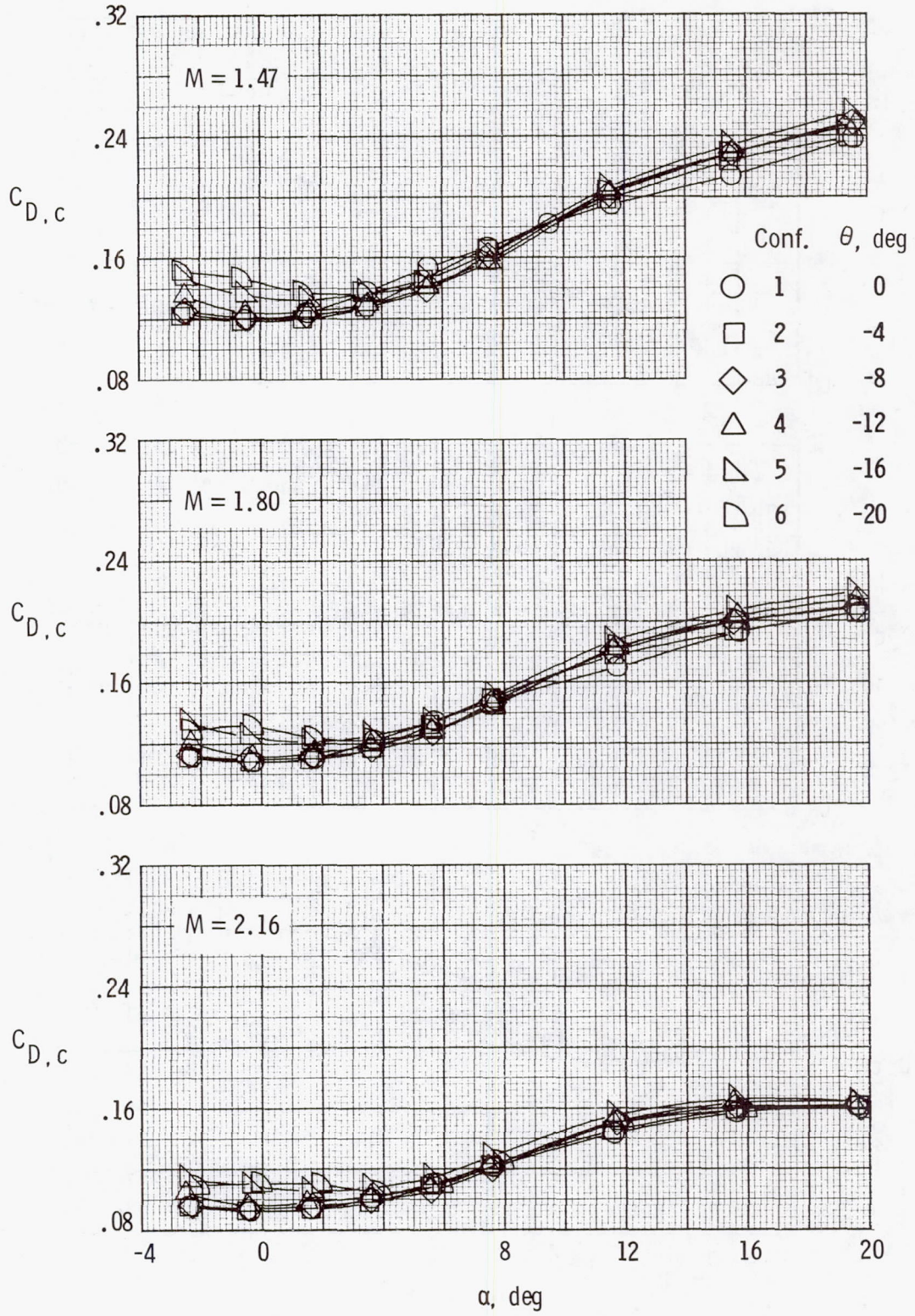

(c) M = 1.47 to 2.16.

Figure 4.- Concluded.

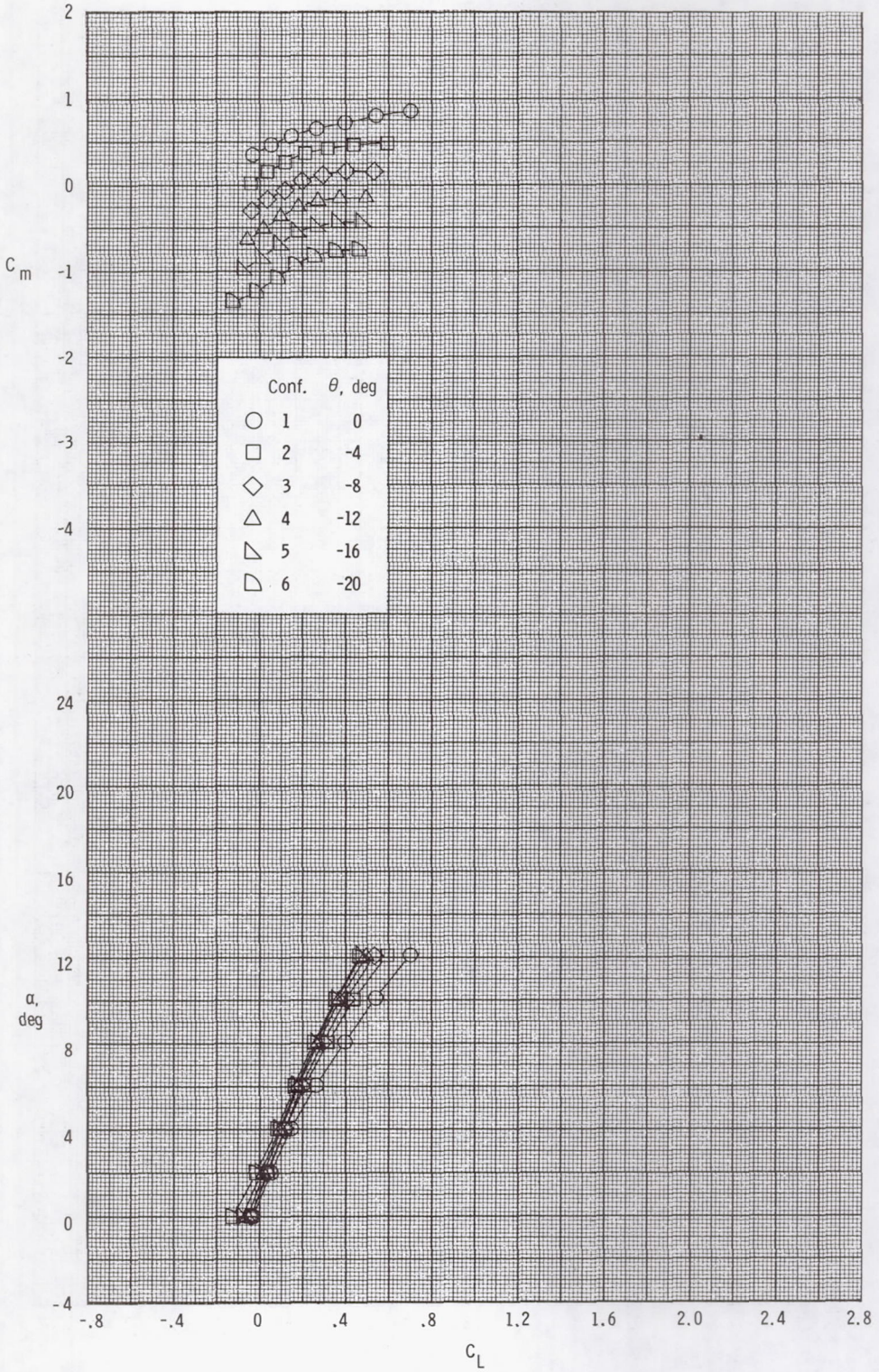

(a) M = 0.60.

Figure 5.- Longitudinal aerodynamic characteristics of the models.

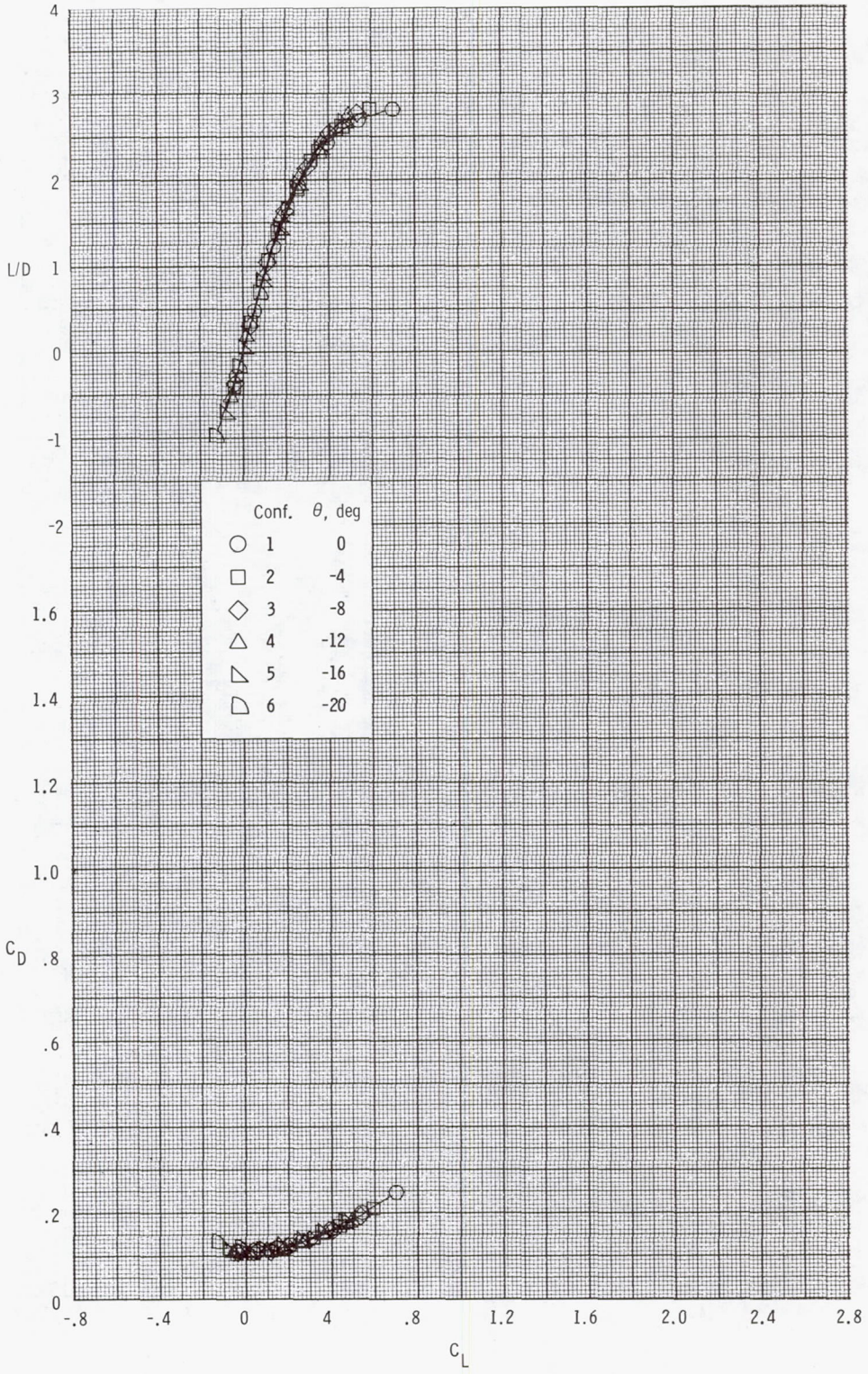

(a) Concluded.

Figure 5.- Continued.

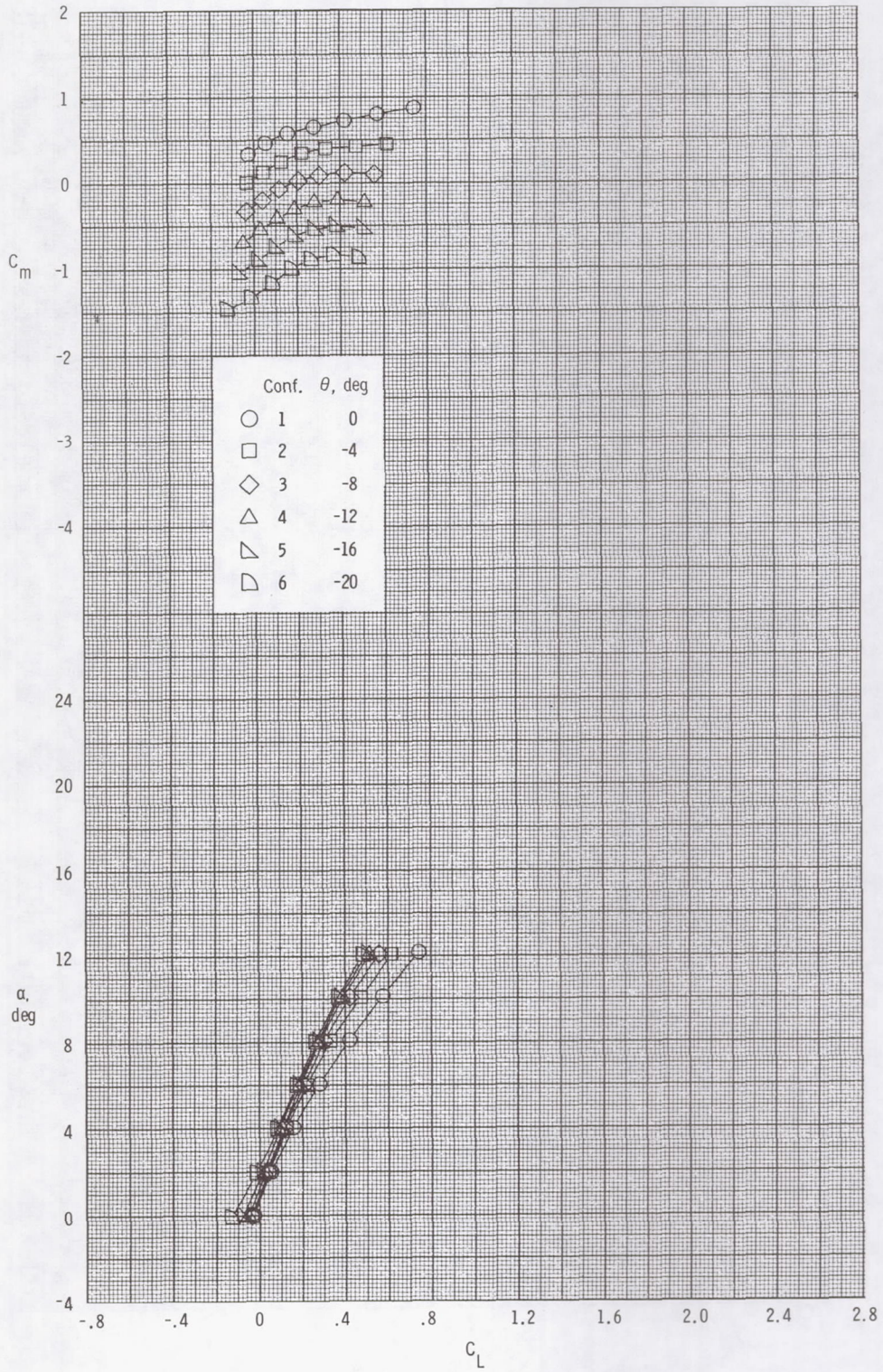

(b) M = 0.80.

Figure 5.- Continued.

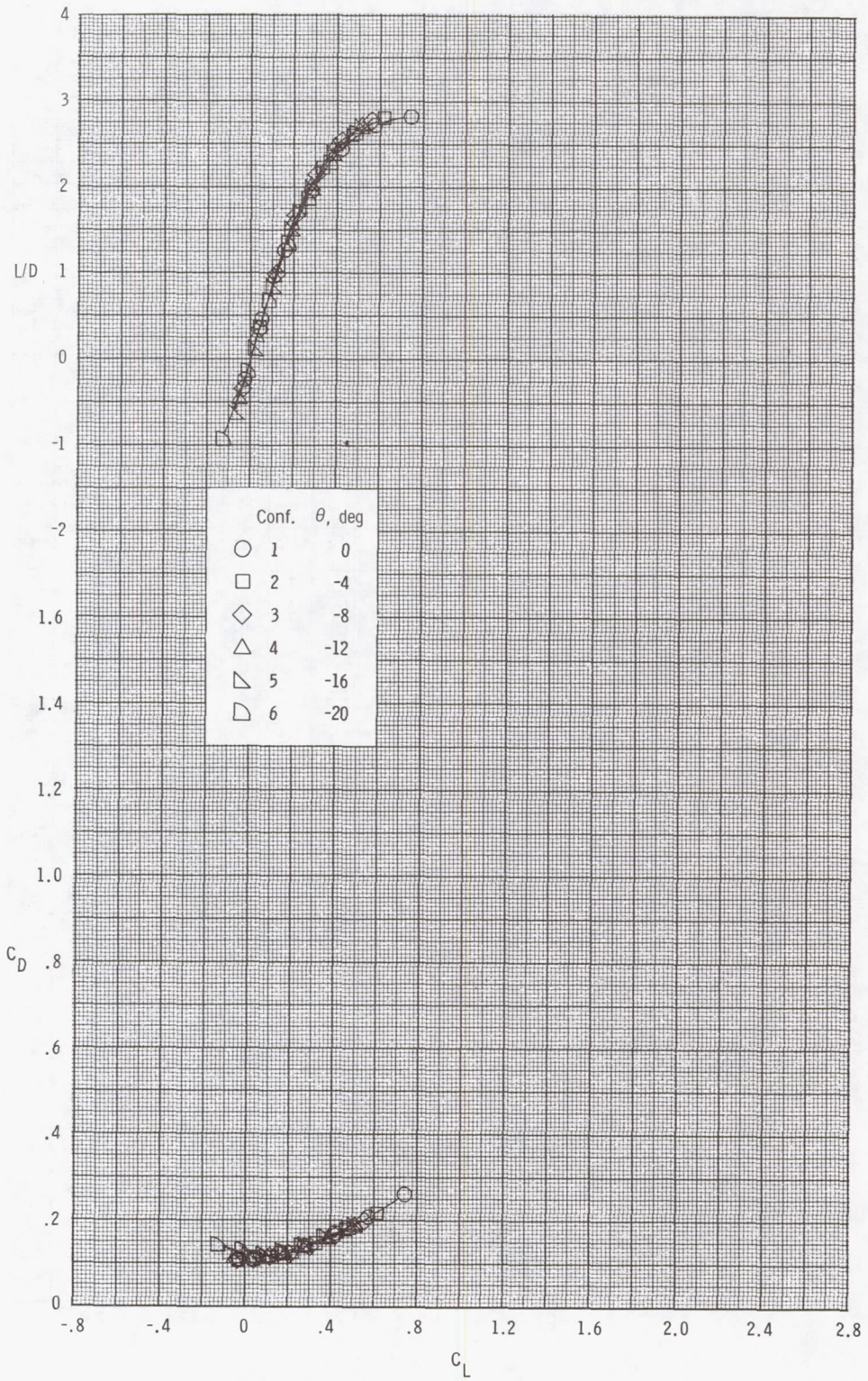

(b) Concluded.

Figure 5.- Continued.

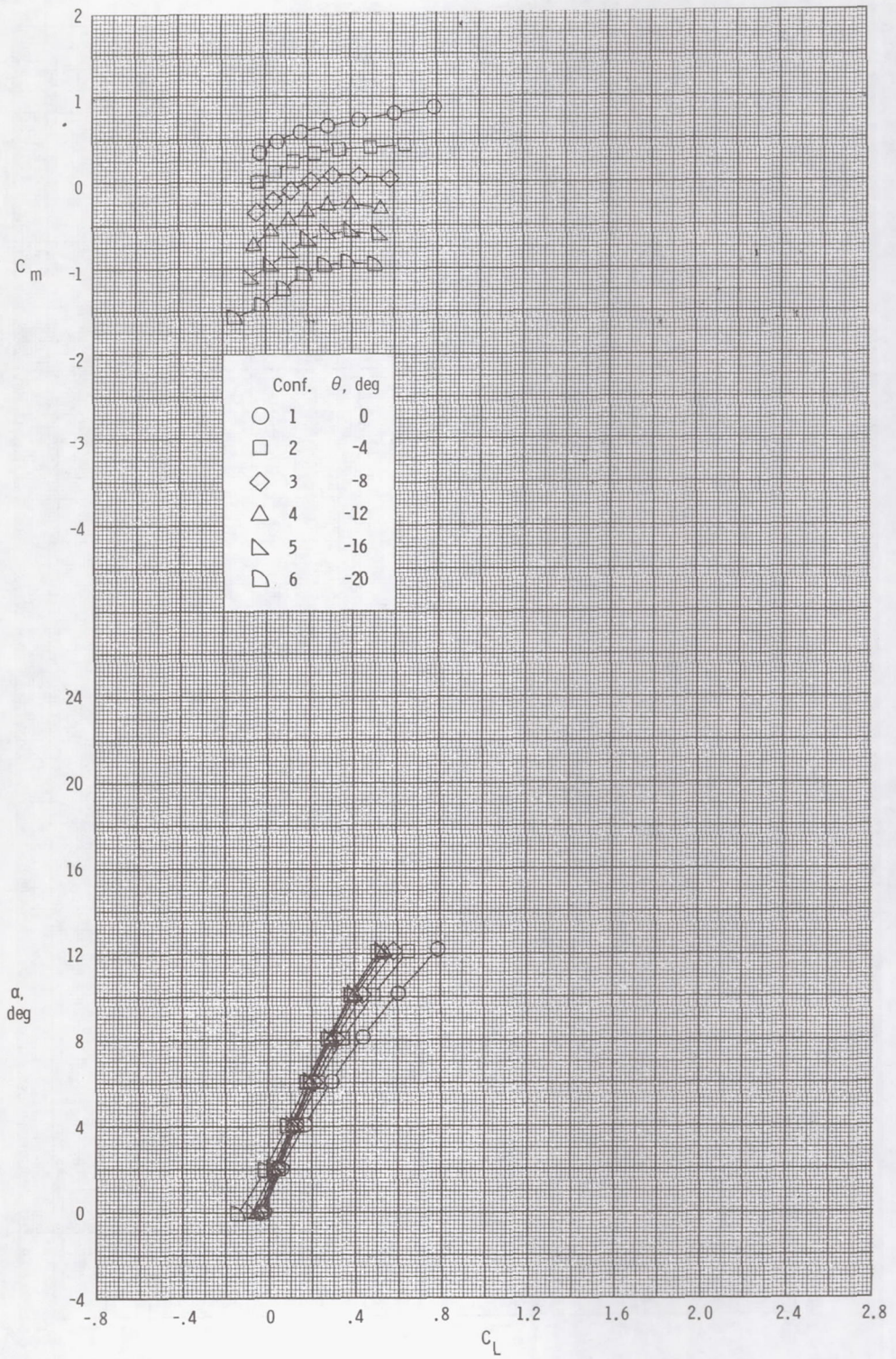

(c) M = 0.90.

Figure 5.- Continued.

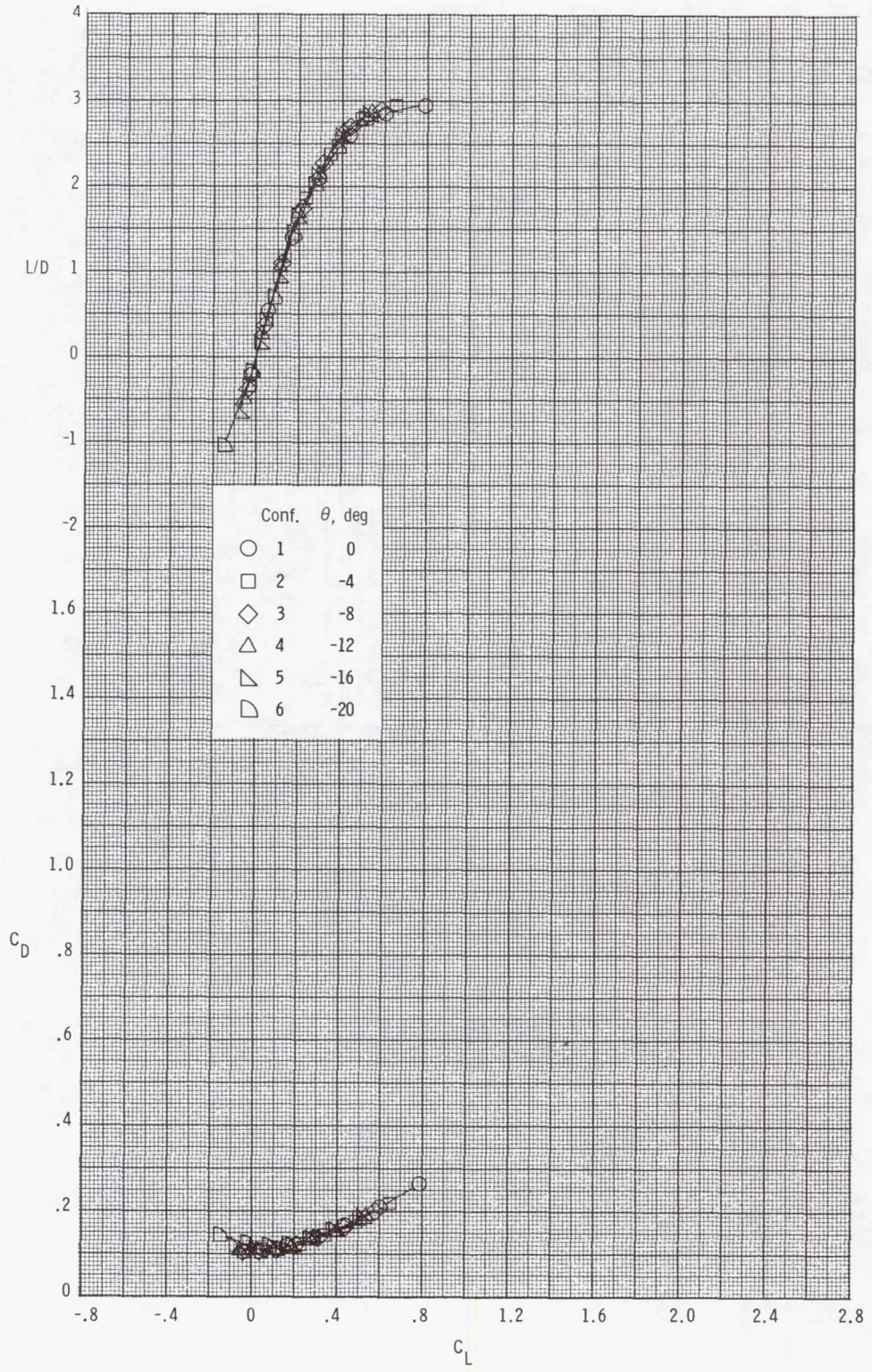

(c) Concluded.

Figure 5.- Continued

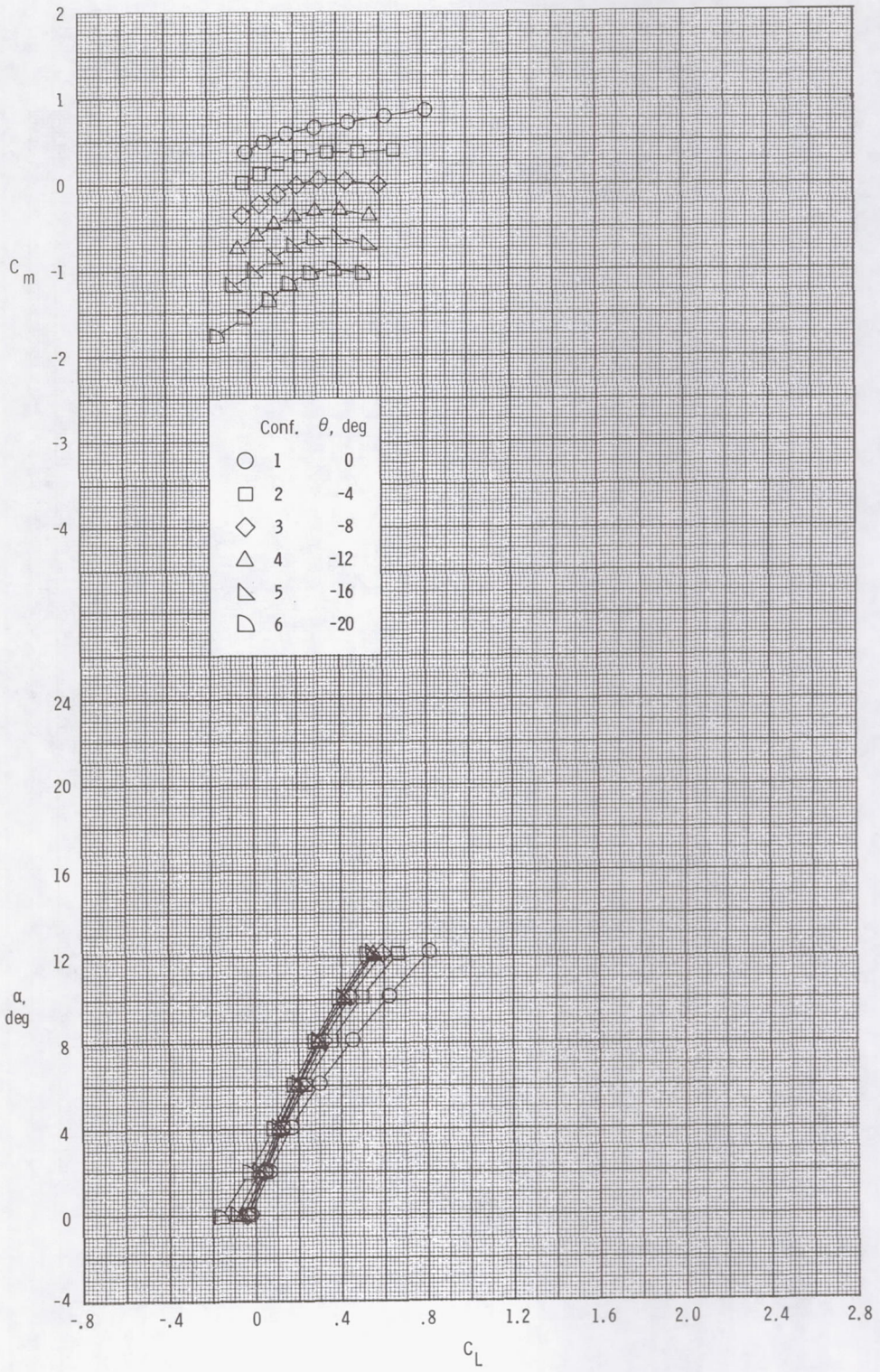

(d) M = 0.95.

Figure 5.- Continued

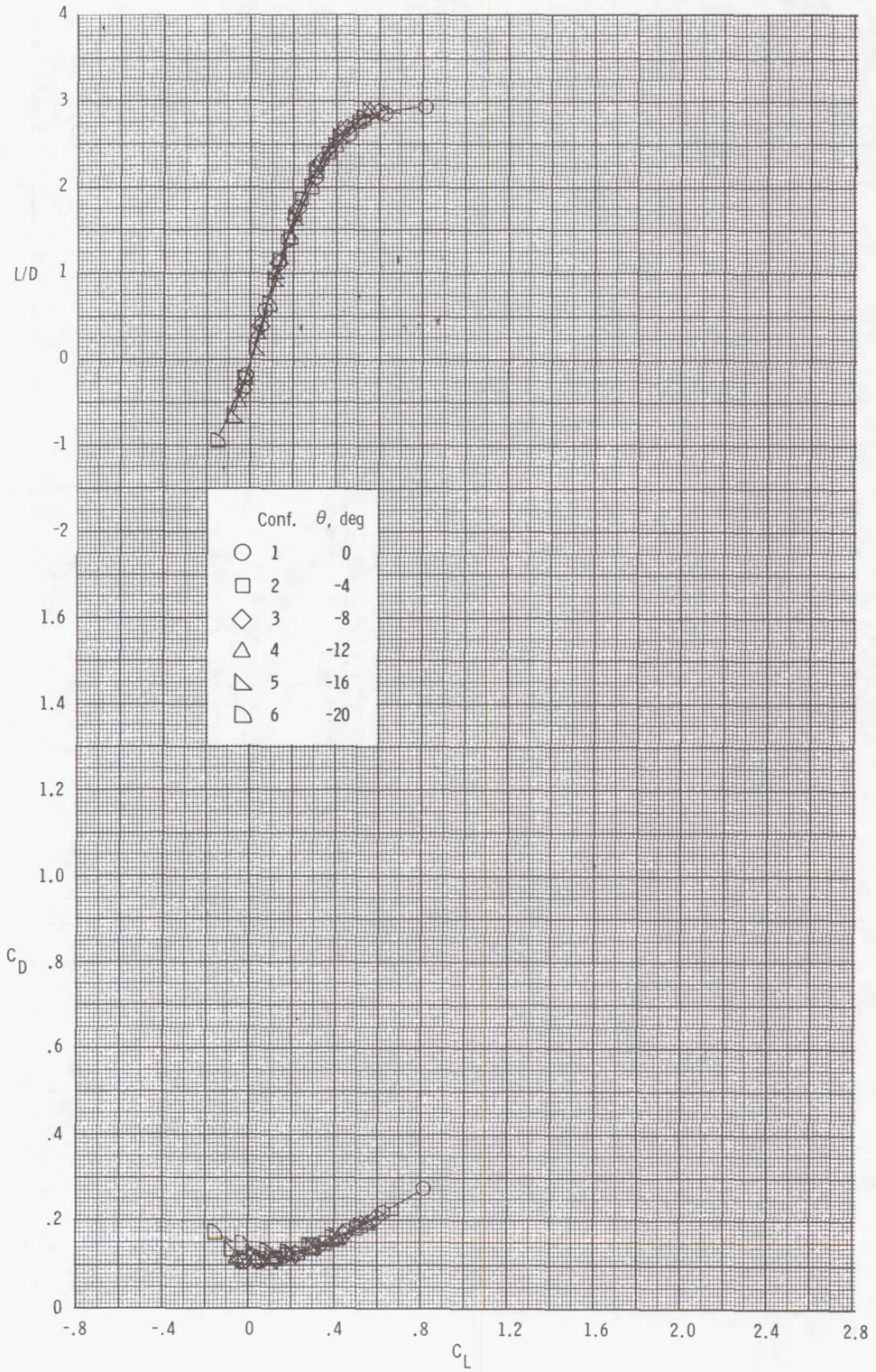

(d) Concluded.

Figure 5.- Continued.

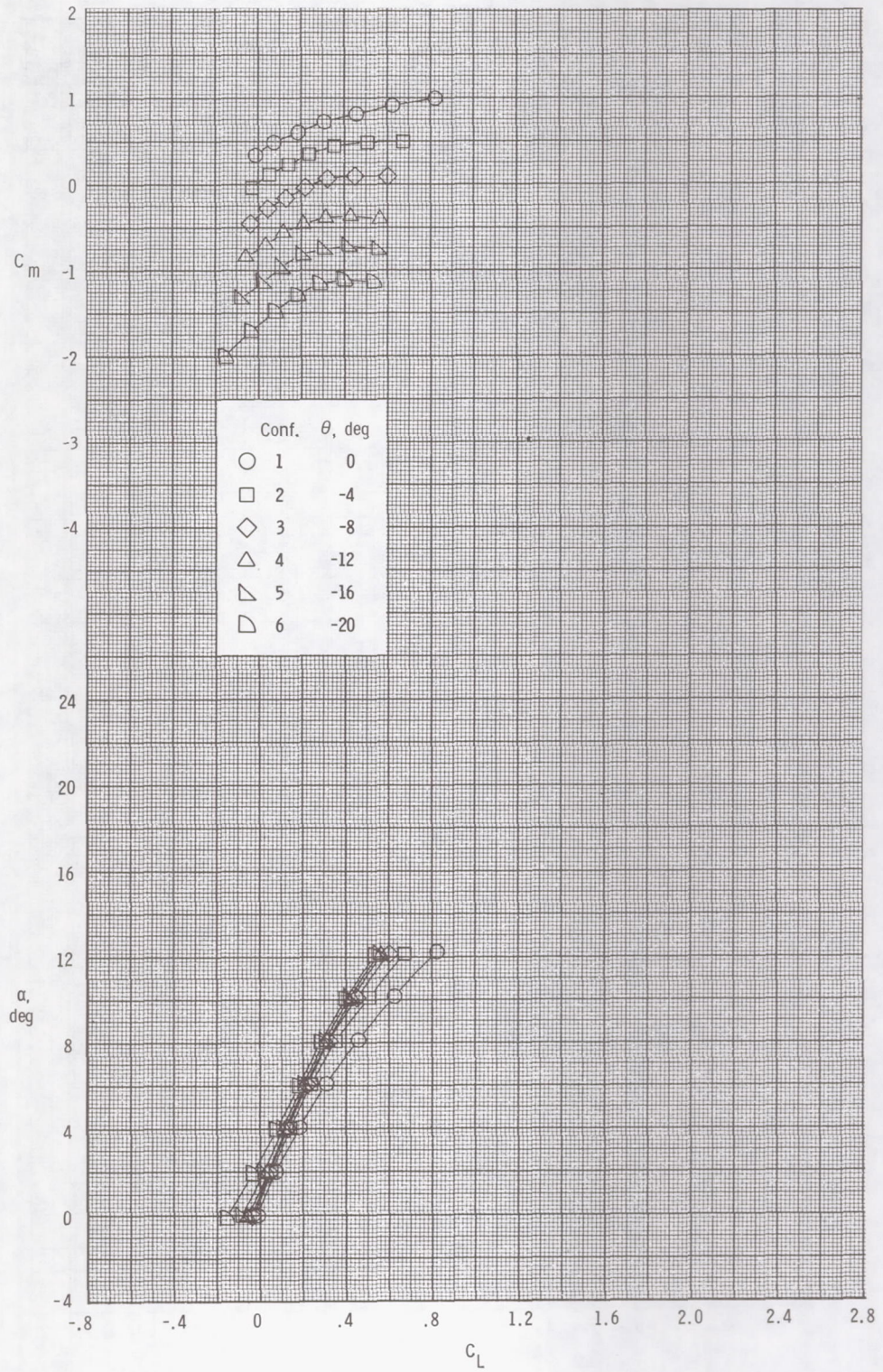

(e) M = 1.10.

Figure 5.- Continued.

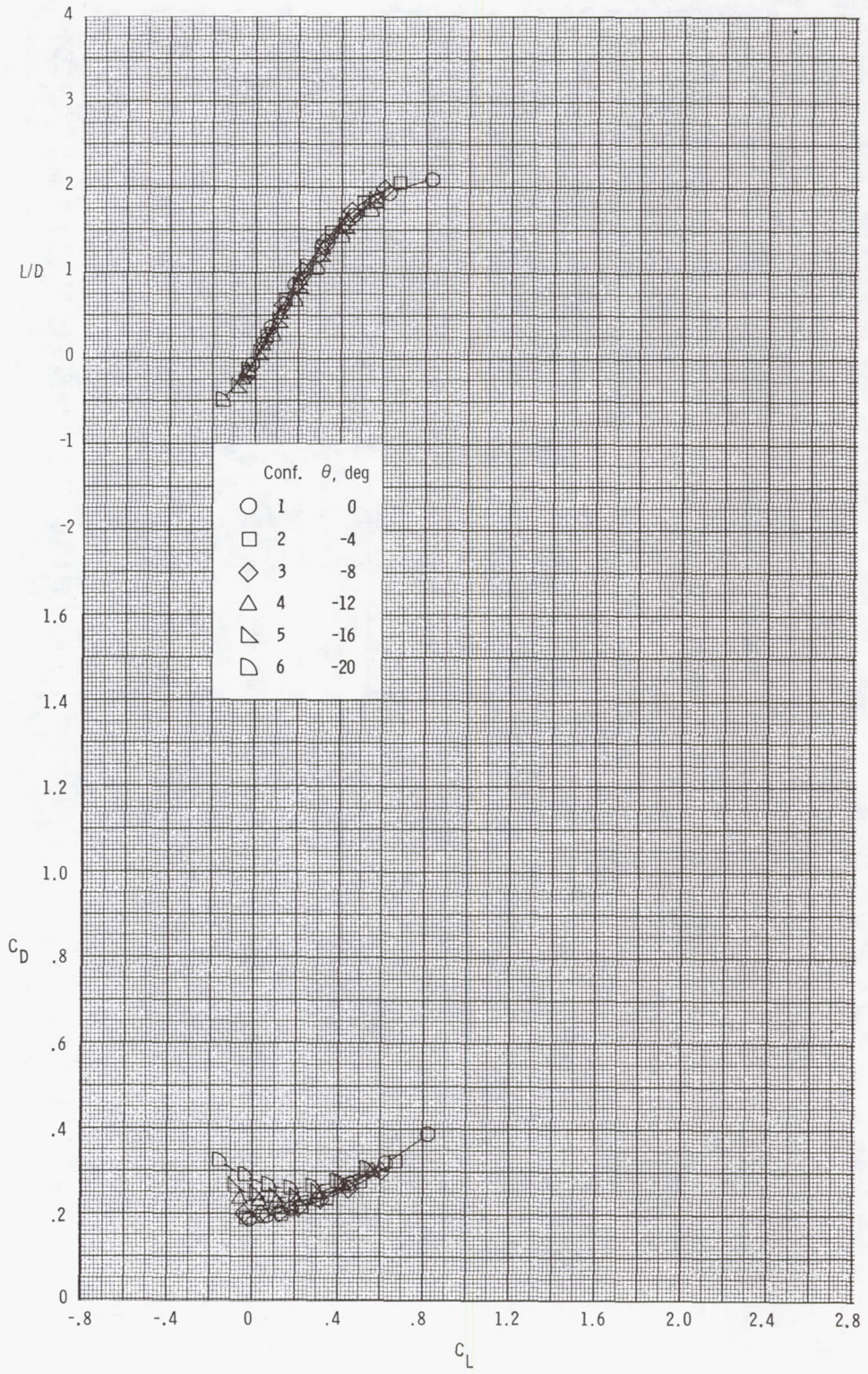

(e) Concluded.

Figure 5.- Continued.

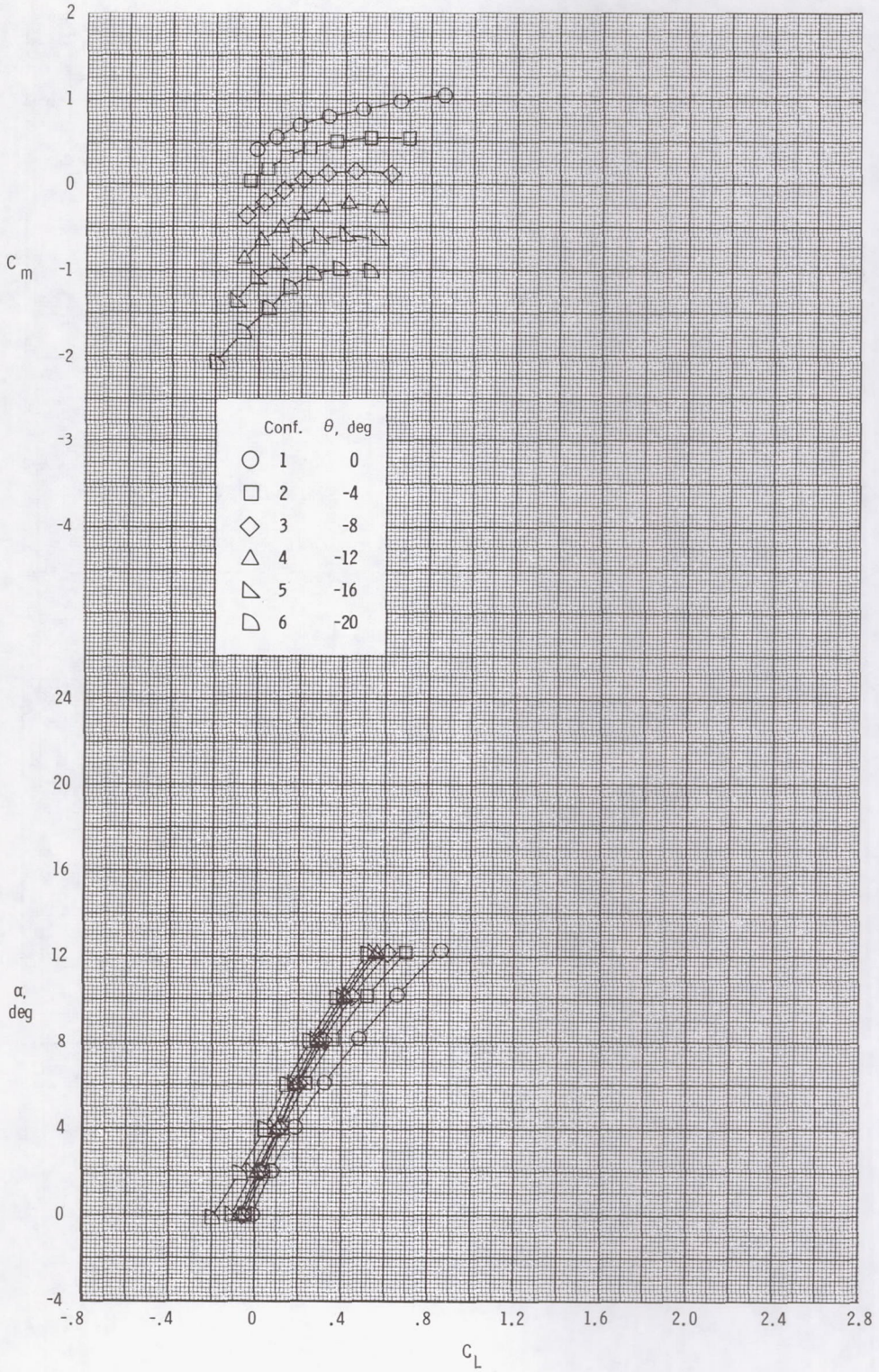

(f) M = 1.20.

Figure 5.- Continued.

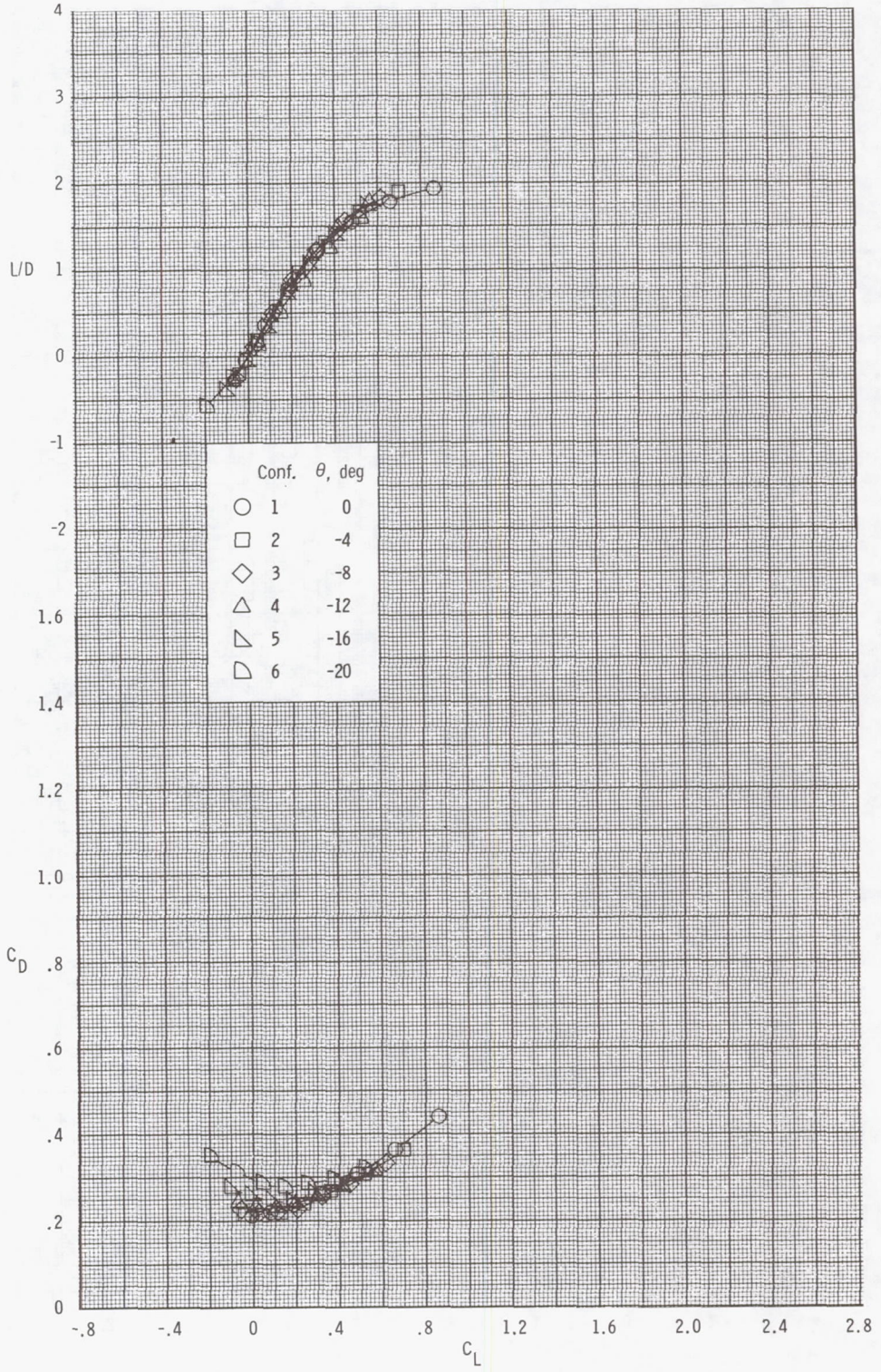

(f) Concluded.

Figure 5.- Continued.

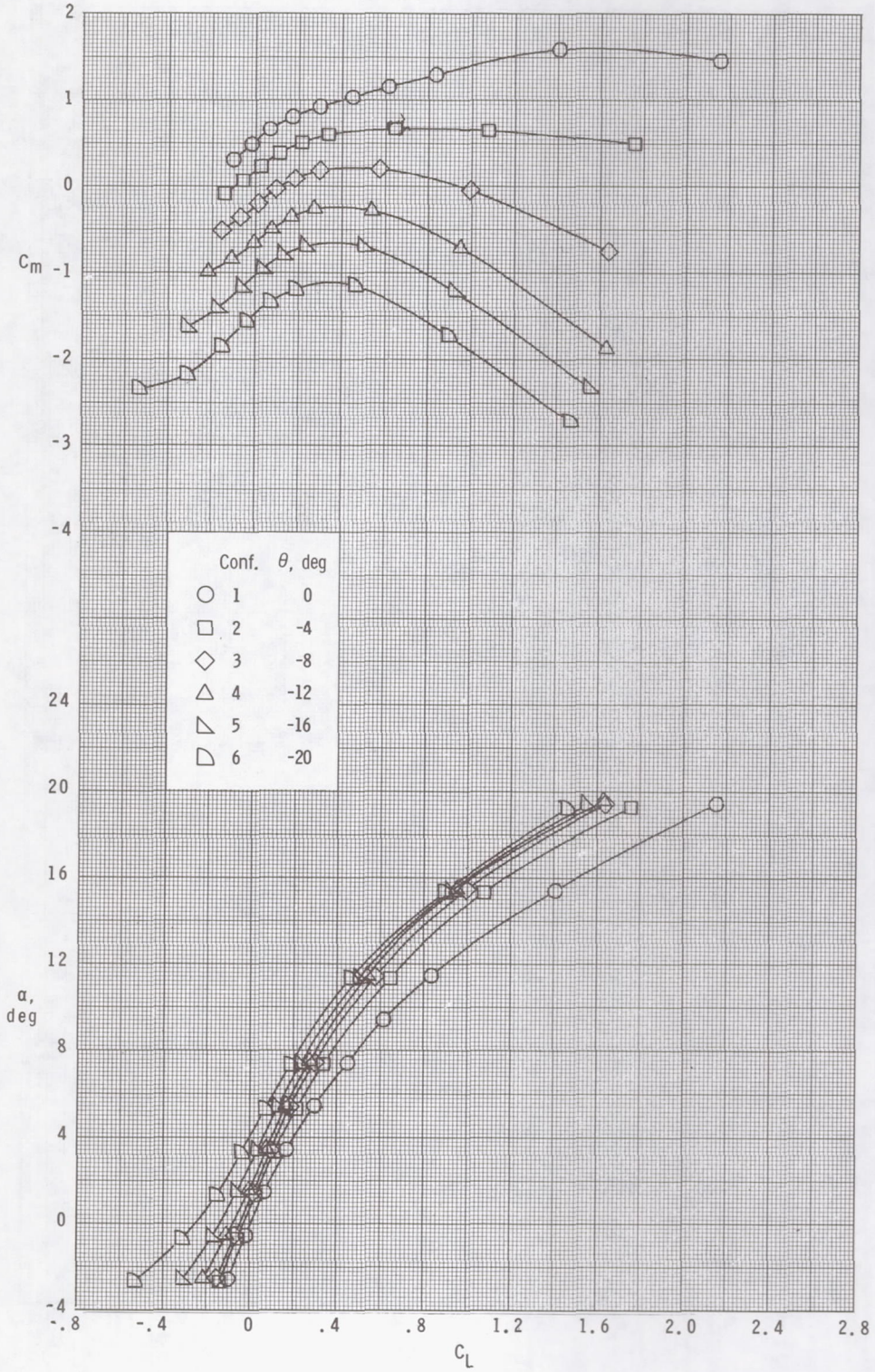

(g) M = 1.47.

Figure 5.- Continued.

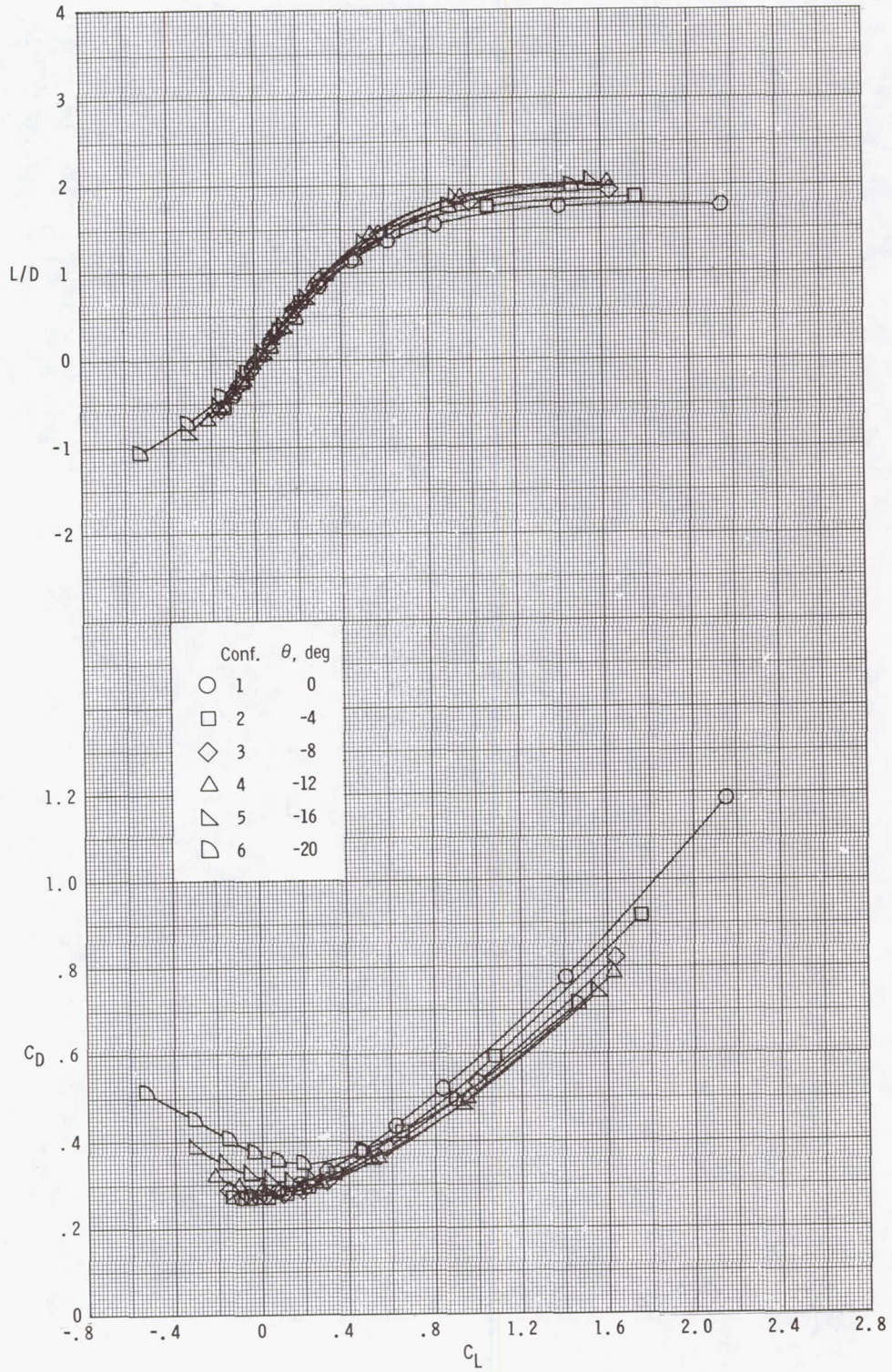

(g) Concluded.

Figure 5.- Continued.

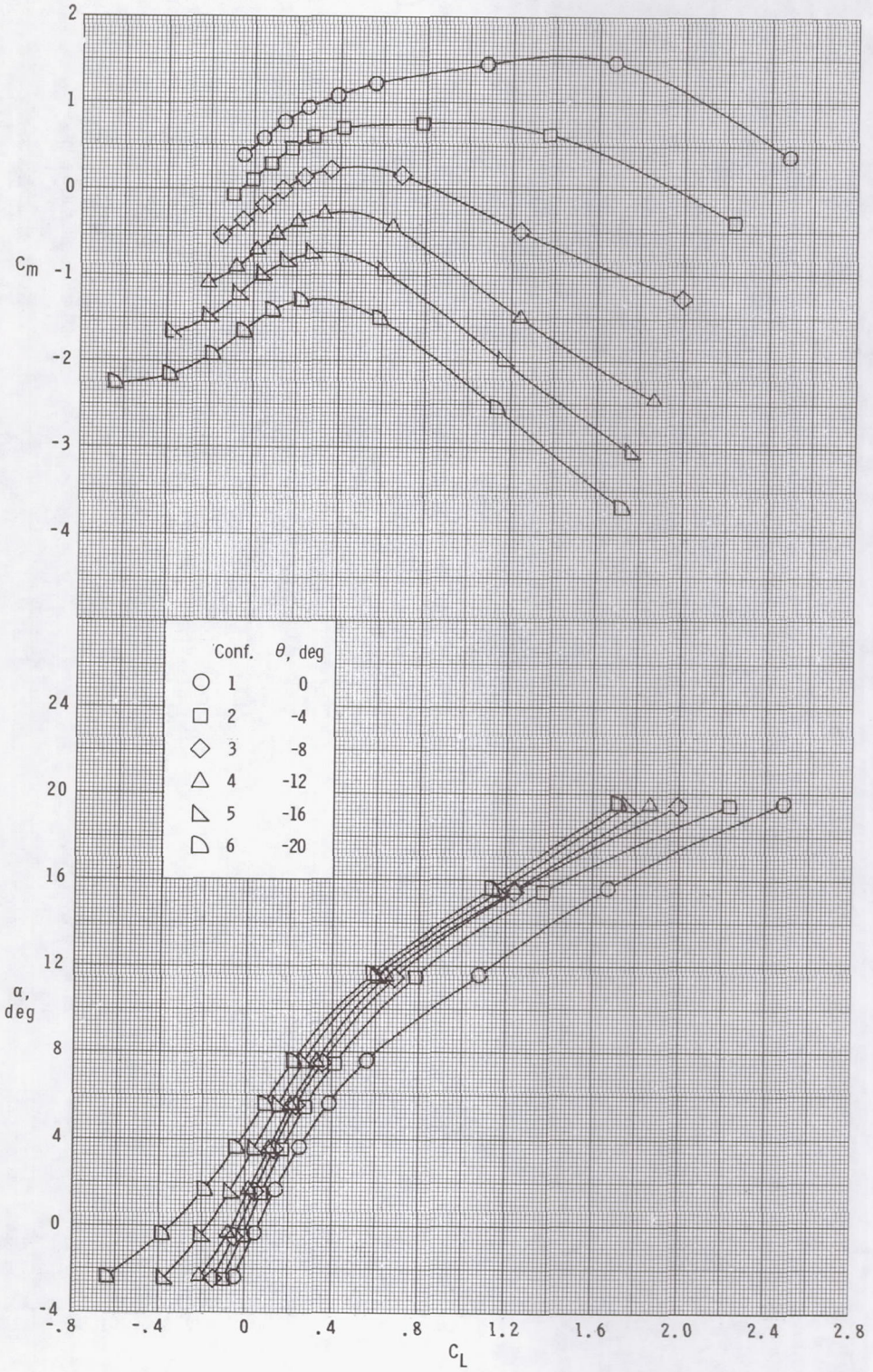

(h) M = 1.80.

Figure 5. - Continued.

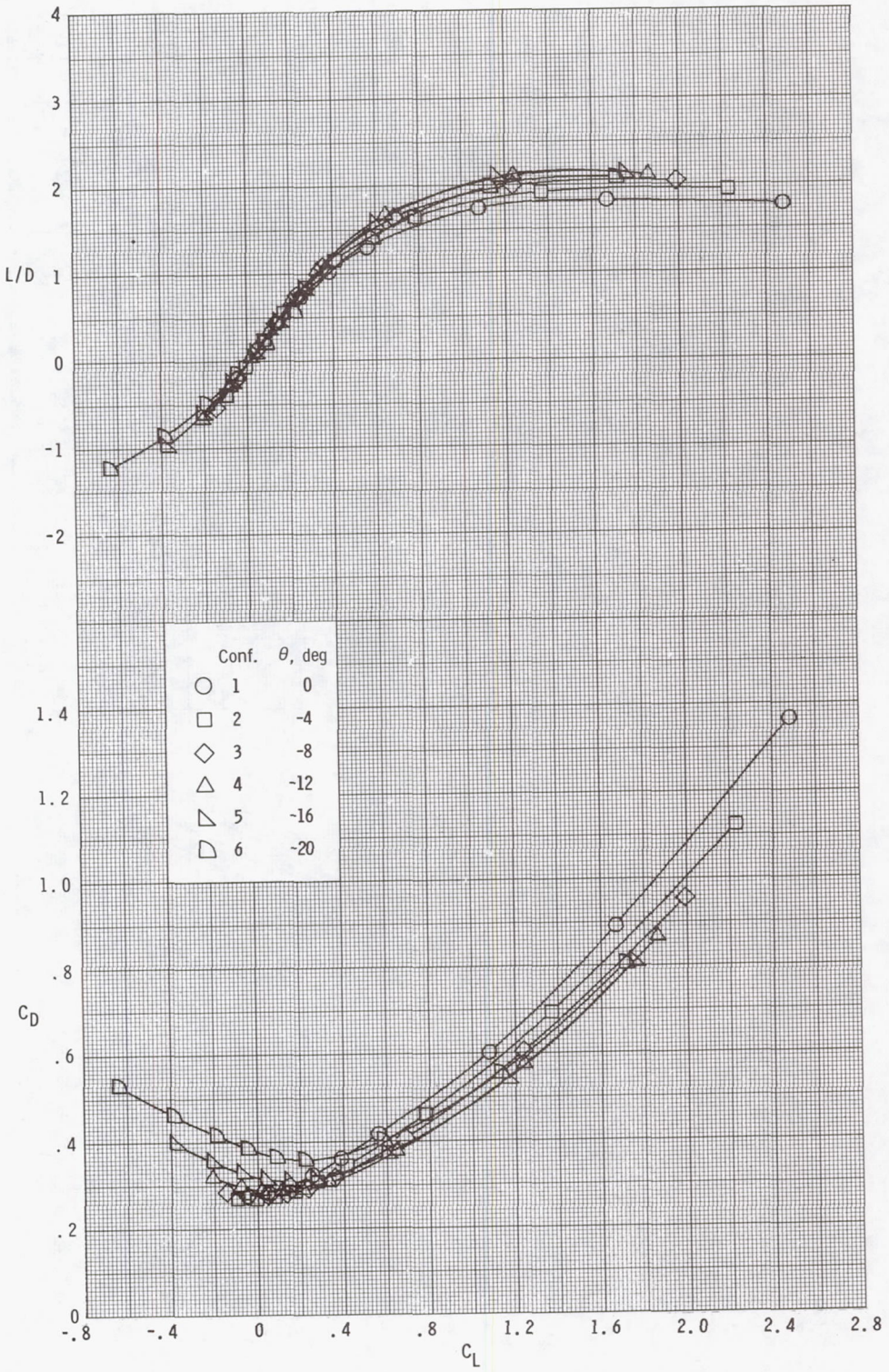

(h) Concluded.

Figure 5.- Continued.

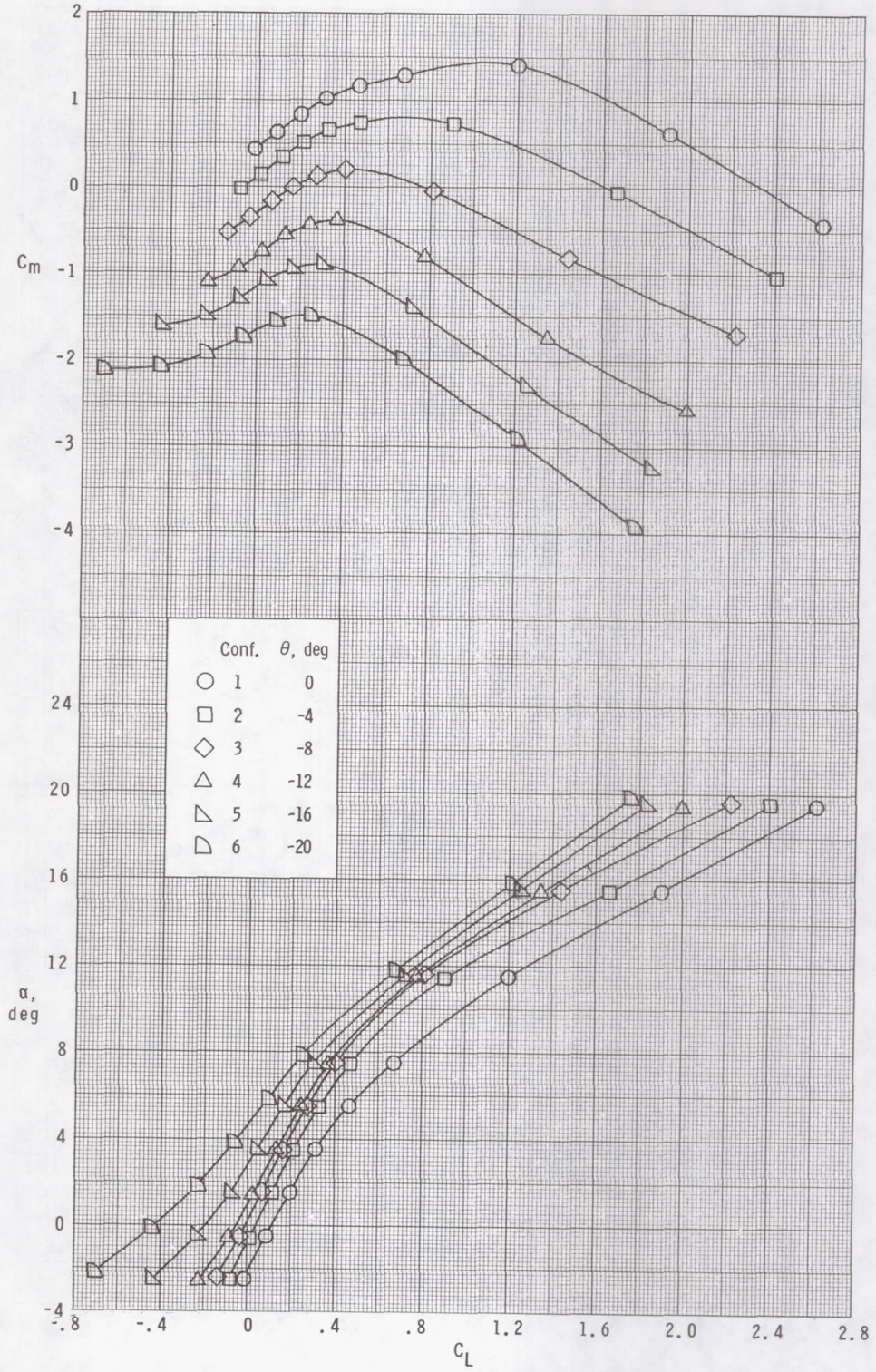

(i) M = 2.16.

Figure 5.- Continued.

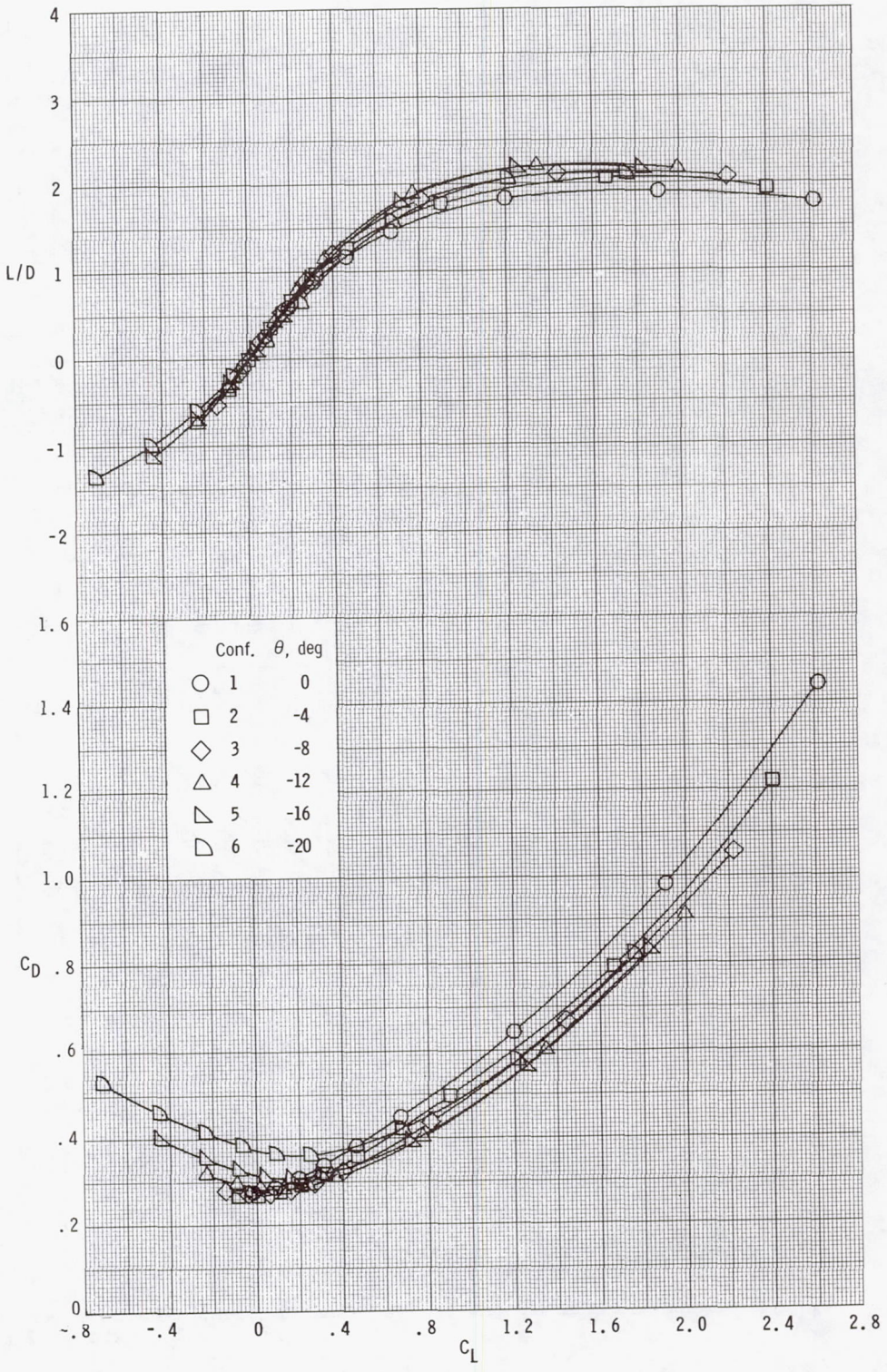

(i) Concluded.

Figure 5.- Concluded.

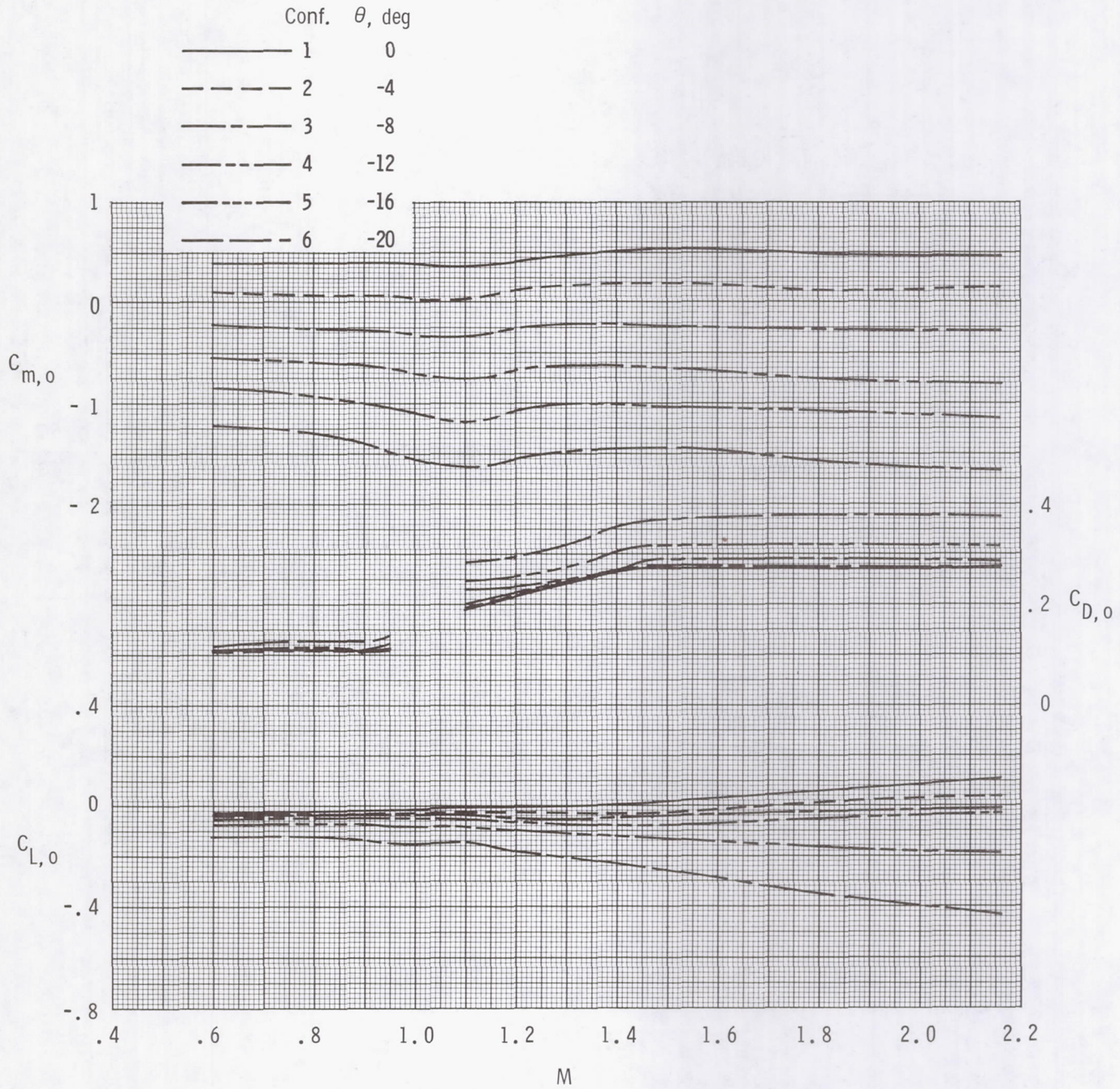

Figure 6.- Variation of longitudinal characteristics with Mach number.

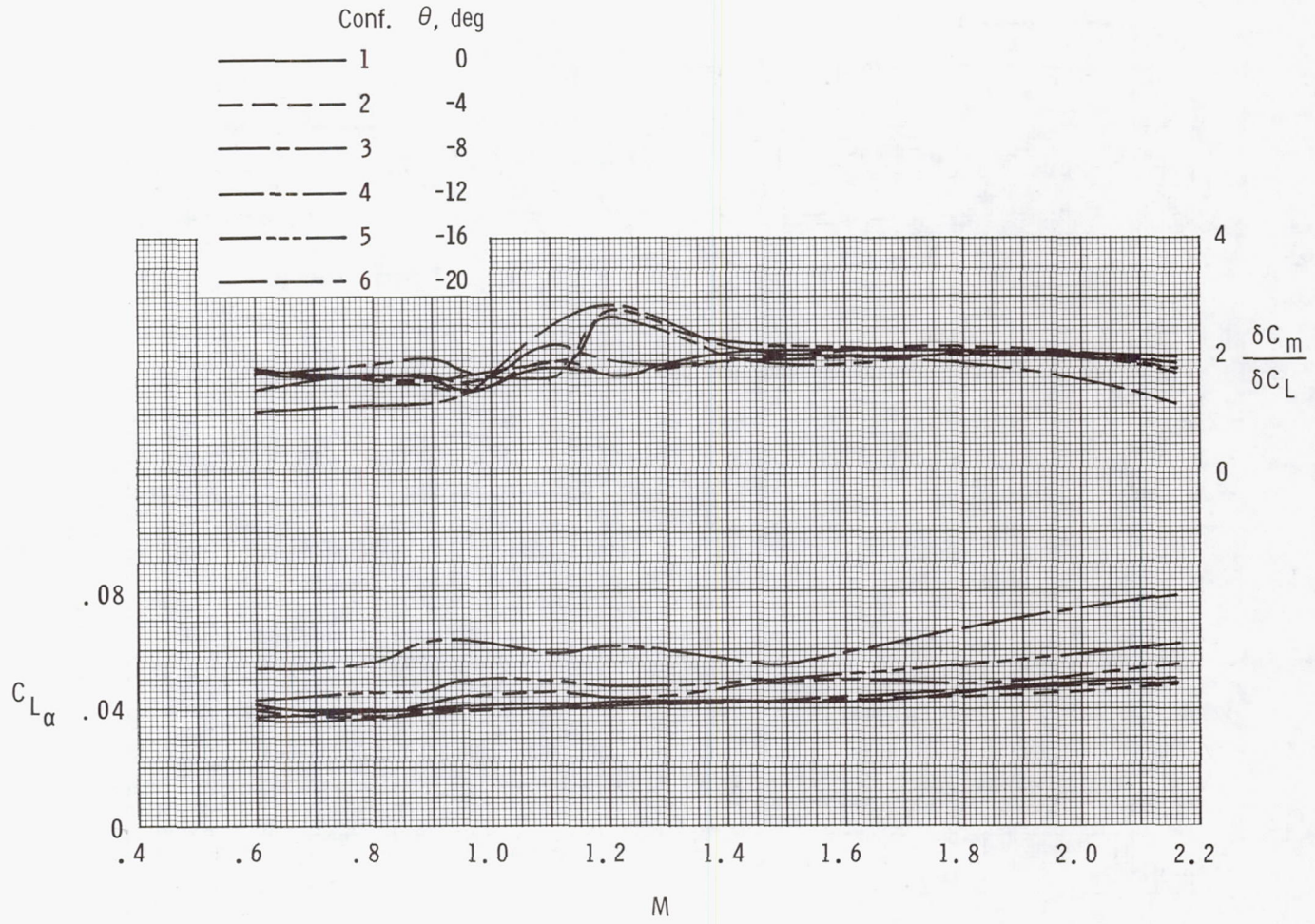

Figure 6.- Concluded.

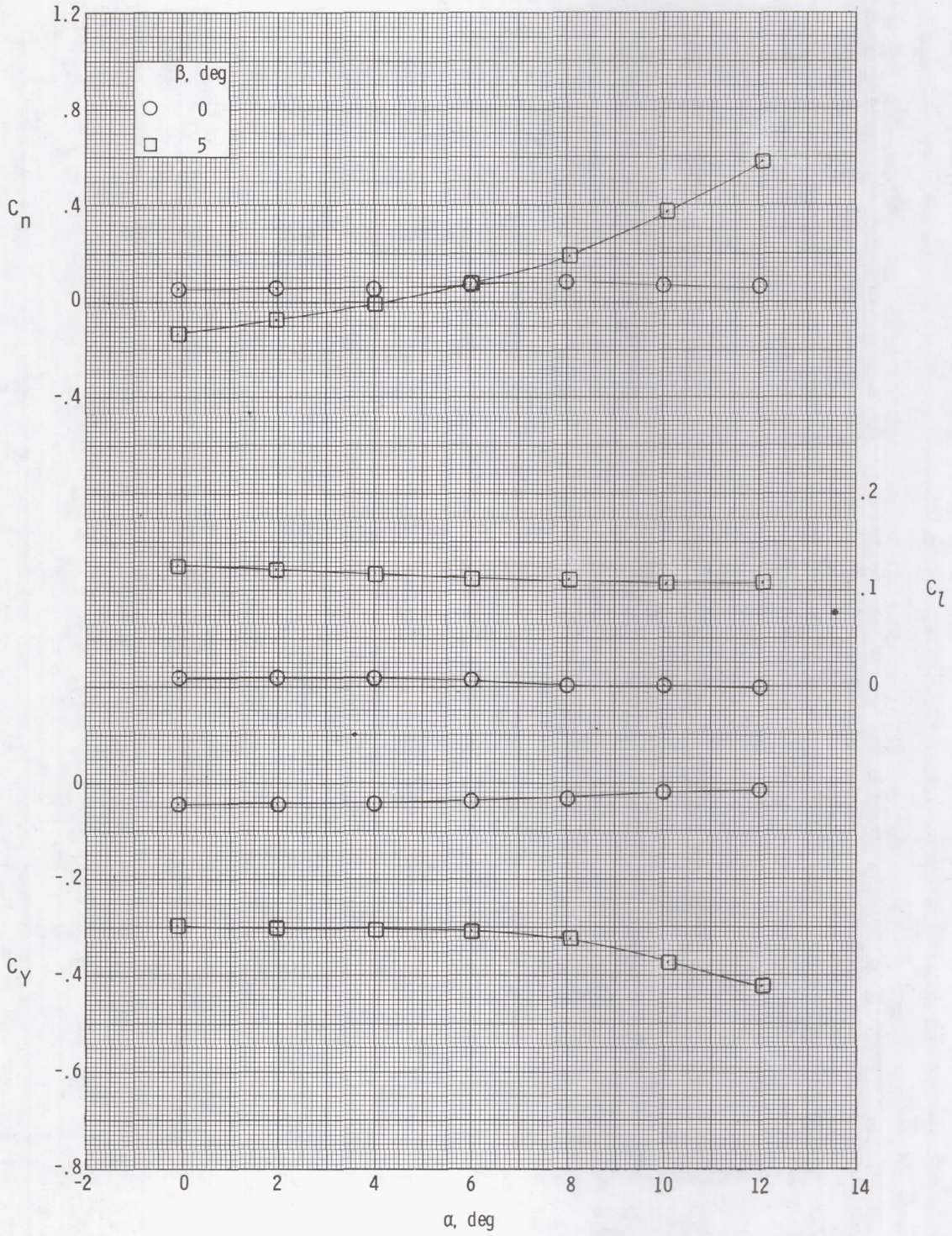

(a) M = 0.60.

Figure 7.- Variation of lateral-directional characteristics at subsonic-transonic speeds (Conf. 6).

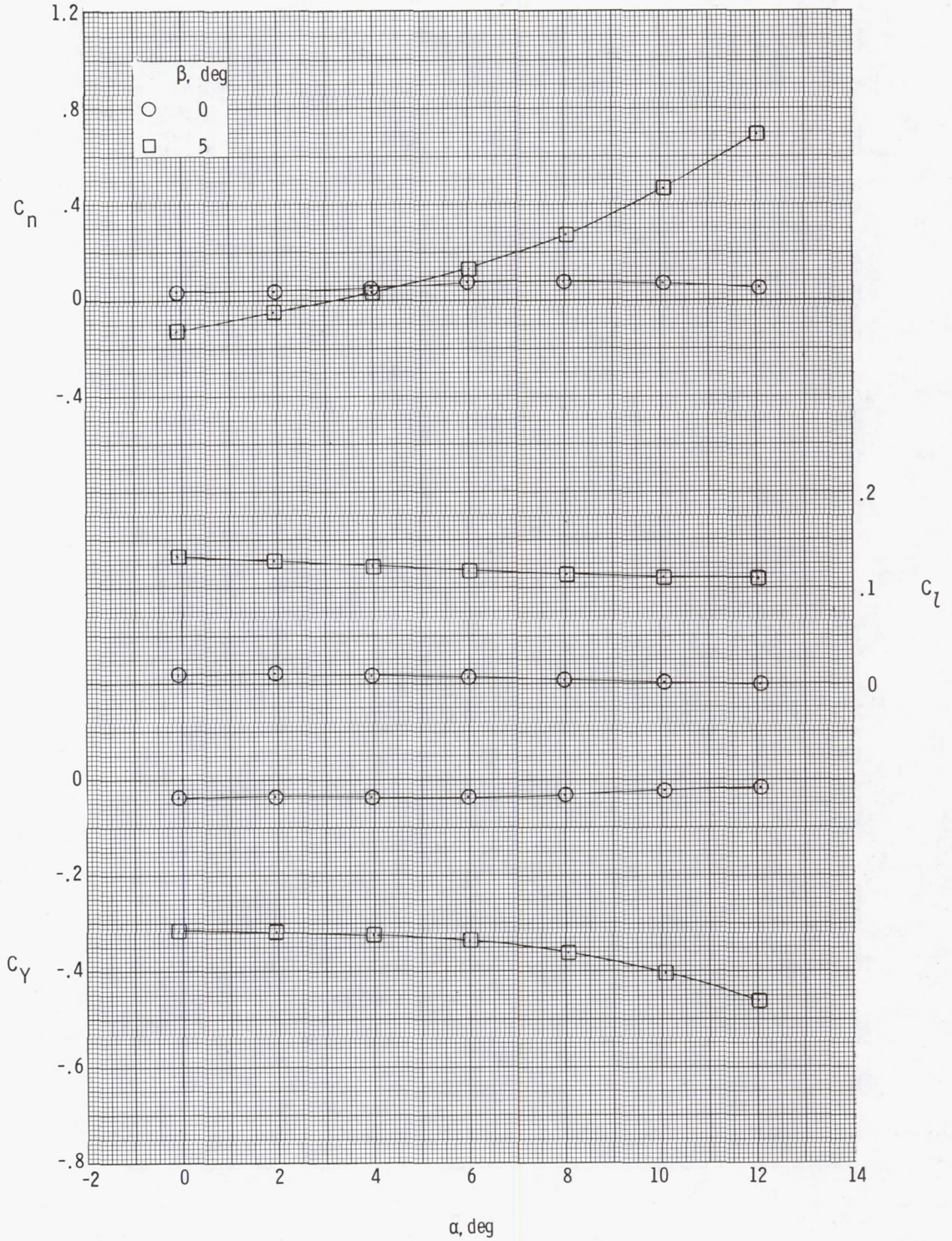

(b) M = 0.80.

Figure 7.- Continued.

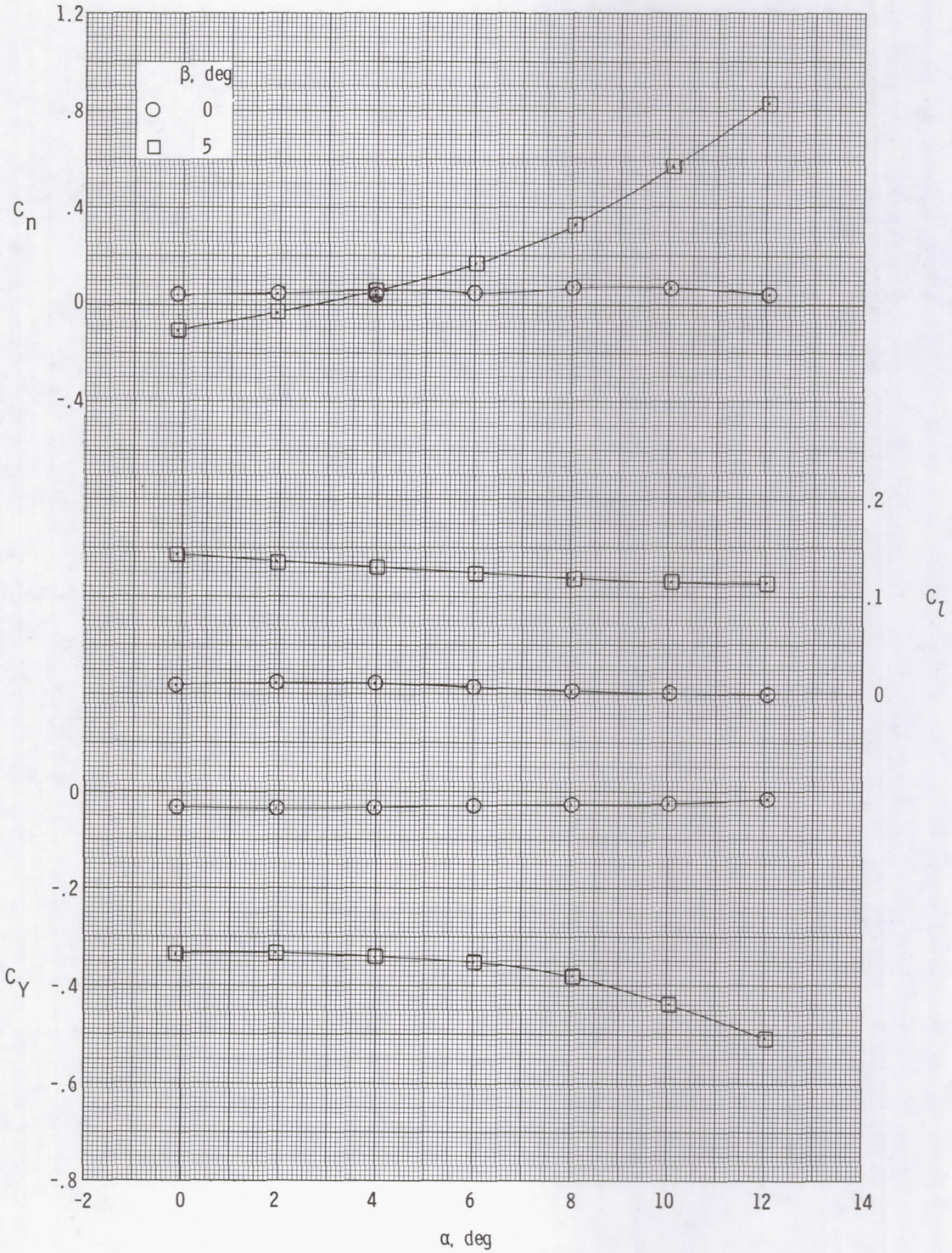

(c) M = 0.90.

Figure 7.- Continued.

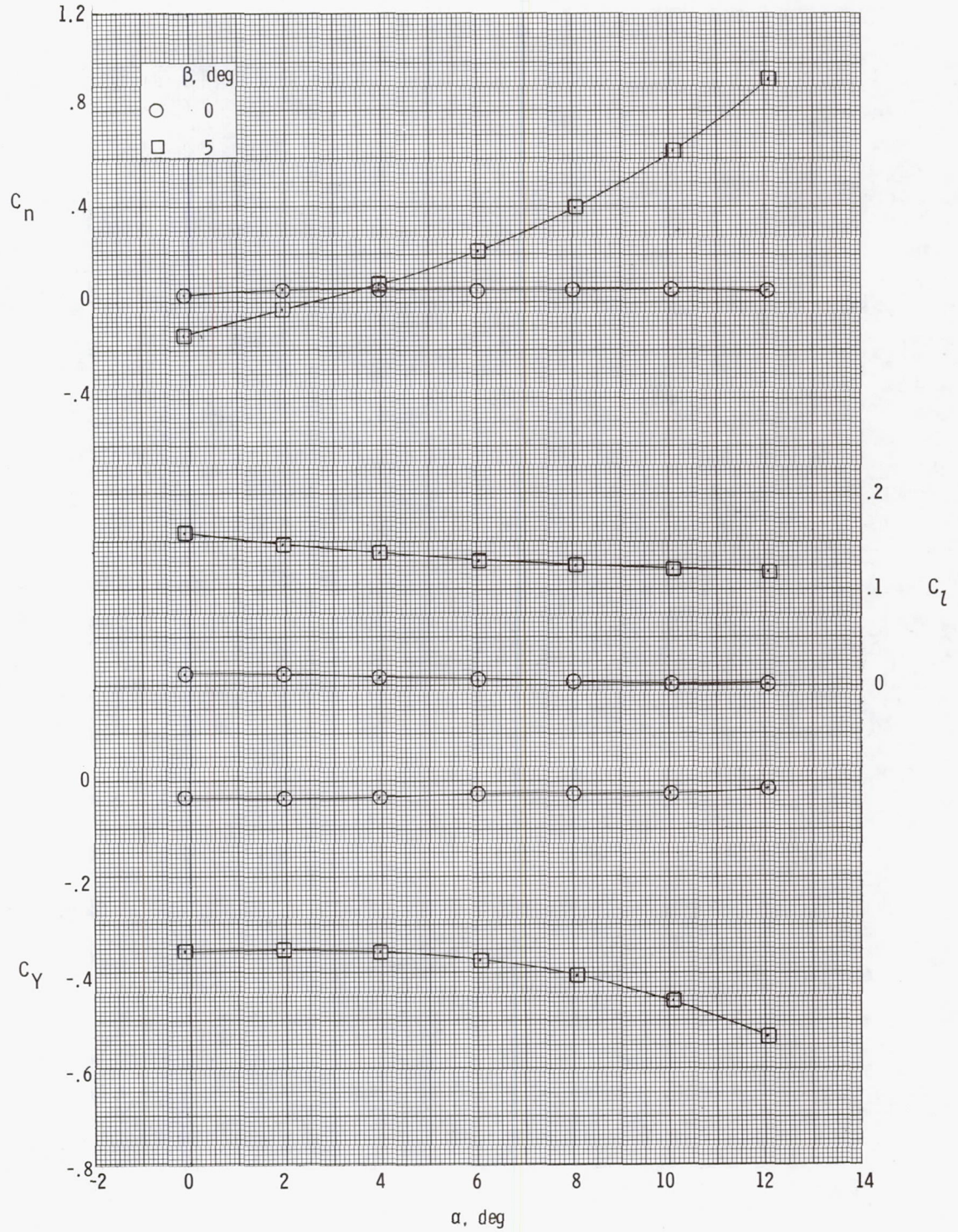

(d) M = 0.95.

Figure 7.- Continued.

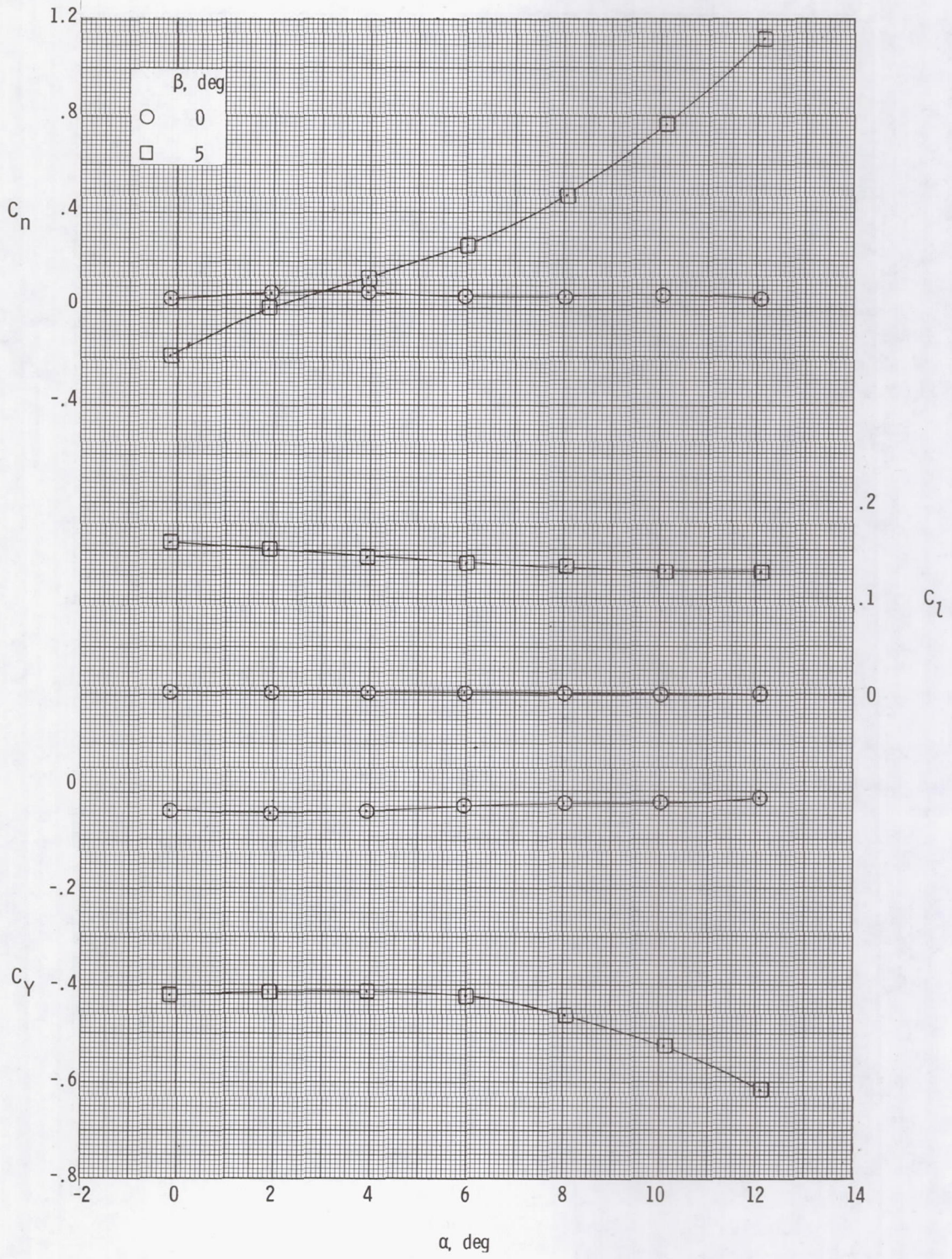

(e) M = 1.10.

Figure 7.- Continued.

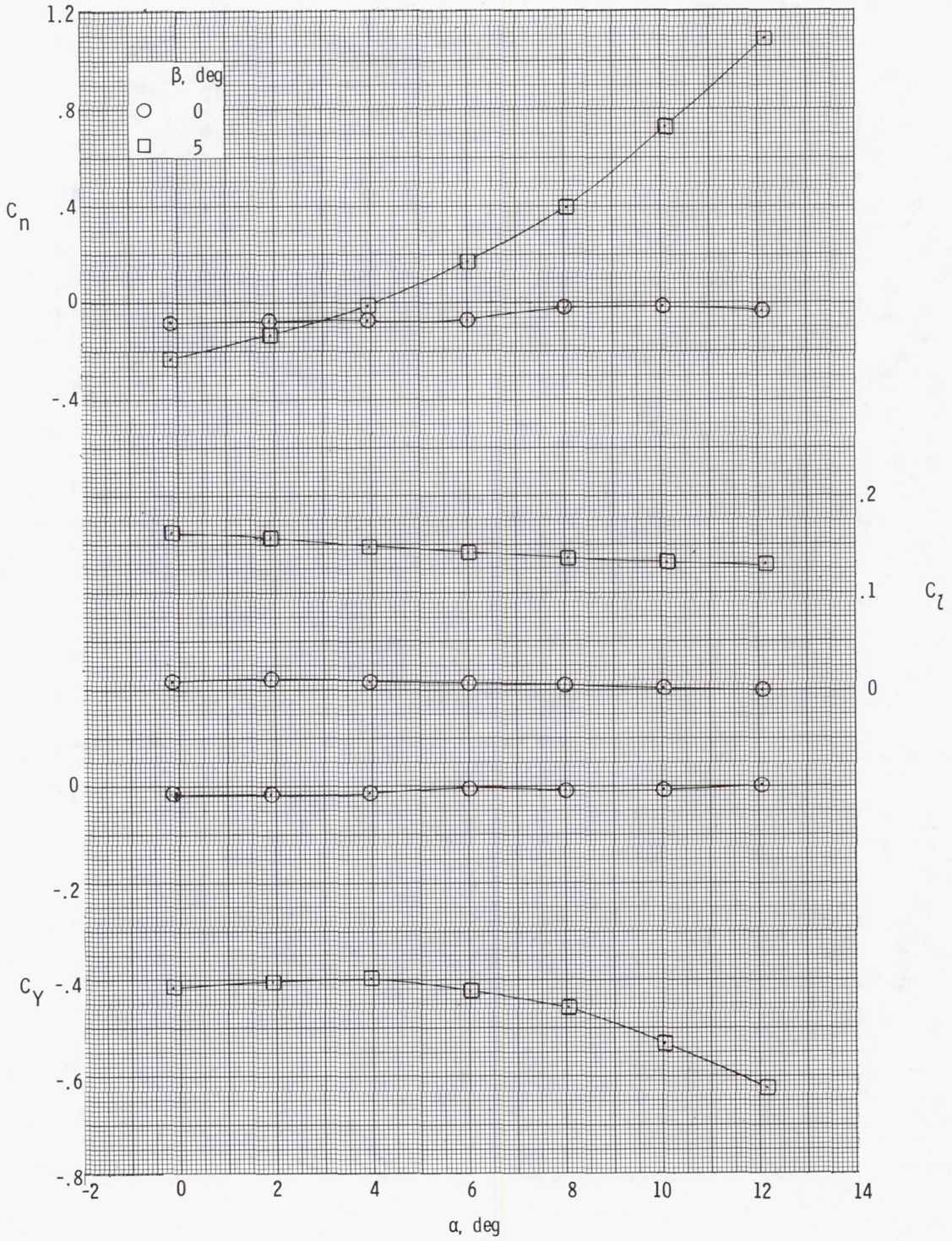

(f) M = 1.20.

Figure 7.- Concluded.

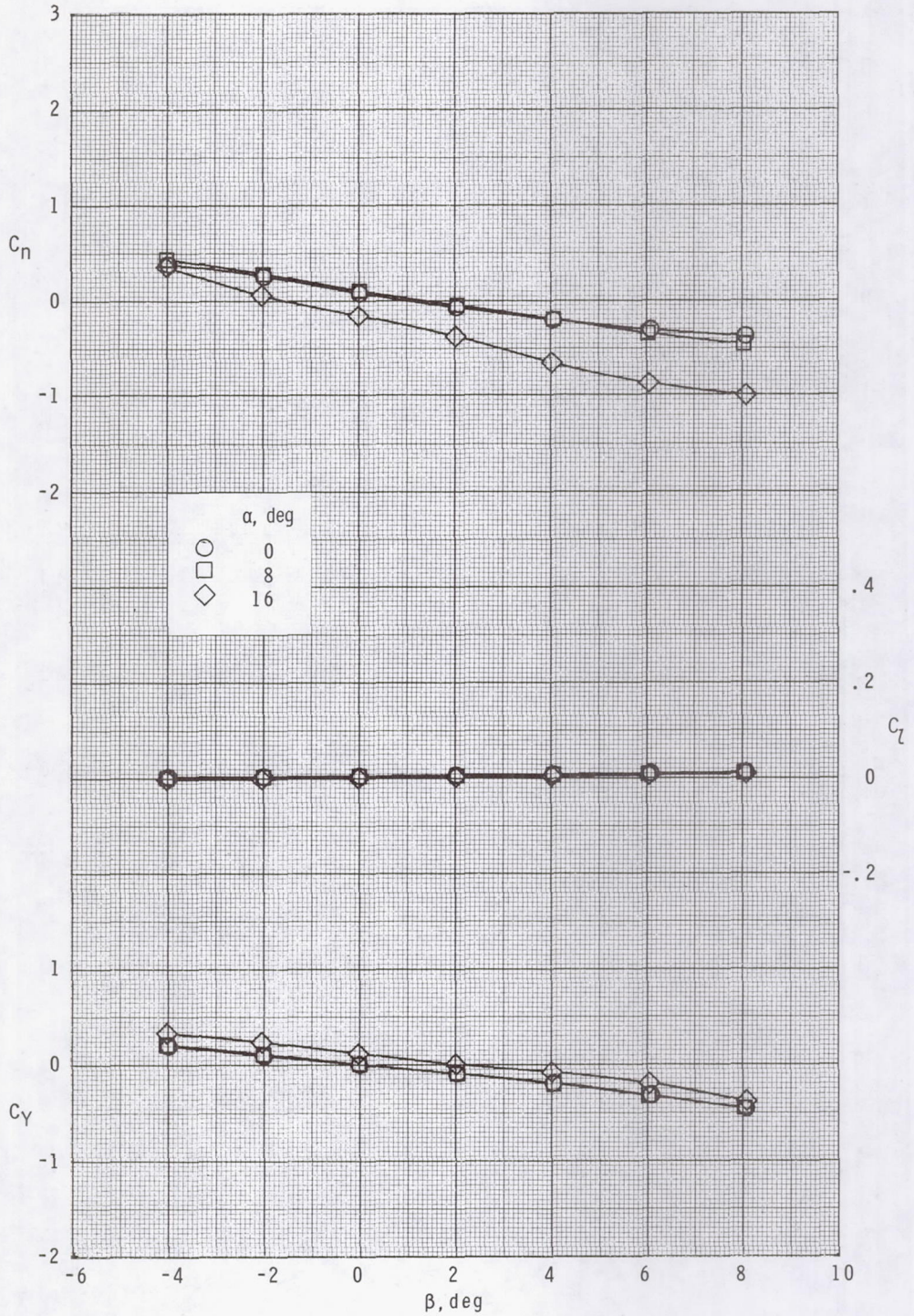

(a) Conf. 2; M = 1.47.

Figure 8.- Variation of lateral-directional characteristics at supersonic speeds.

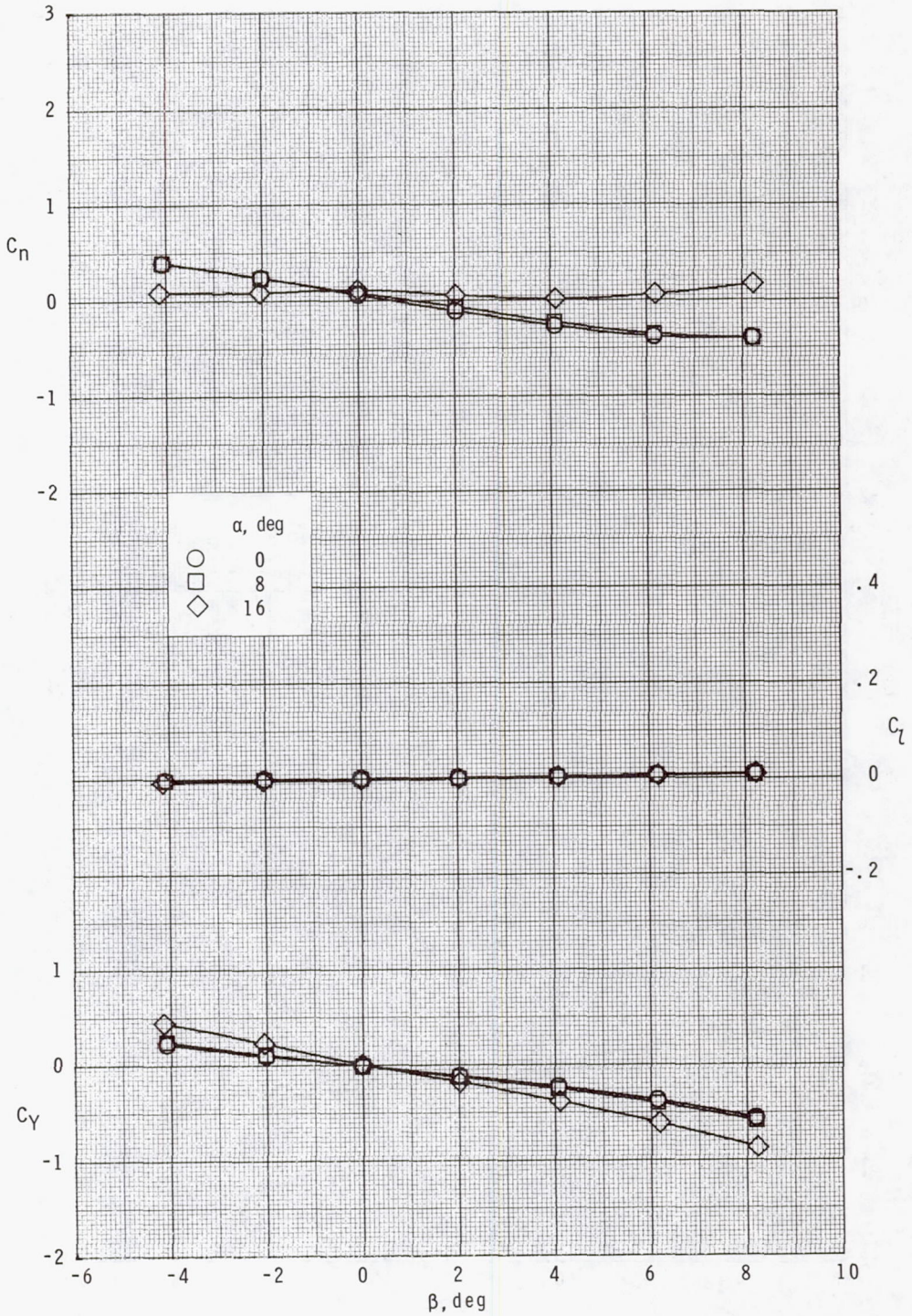

(b) Conf. 2; M = 2.16.

Figure 8.- Continued.

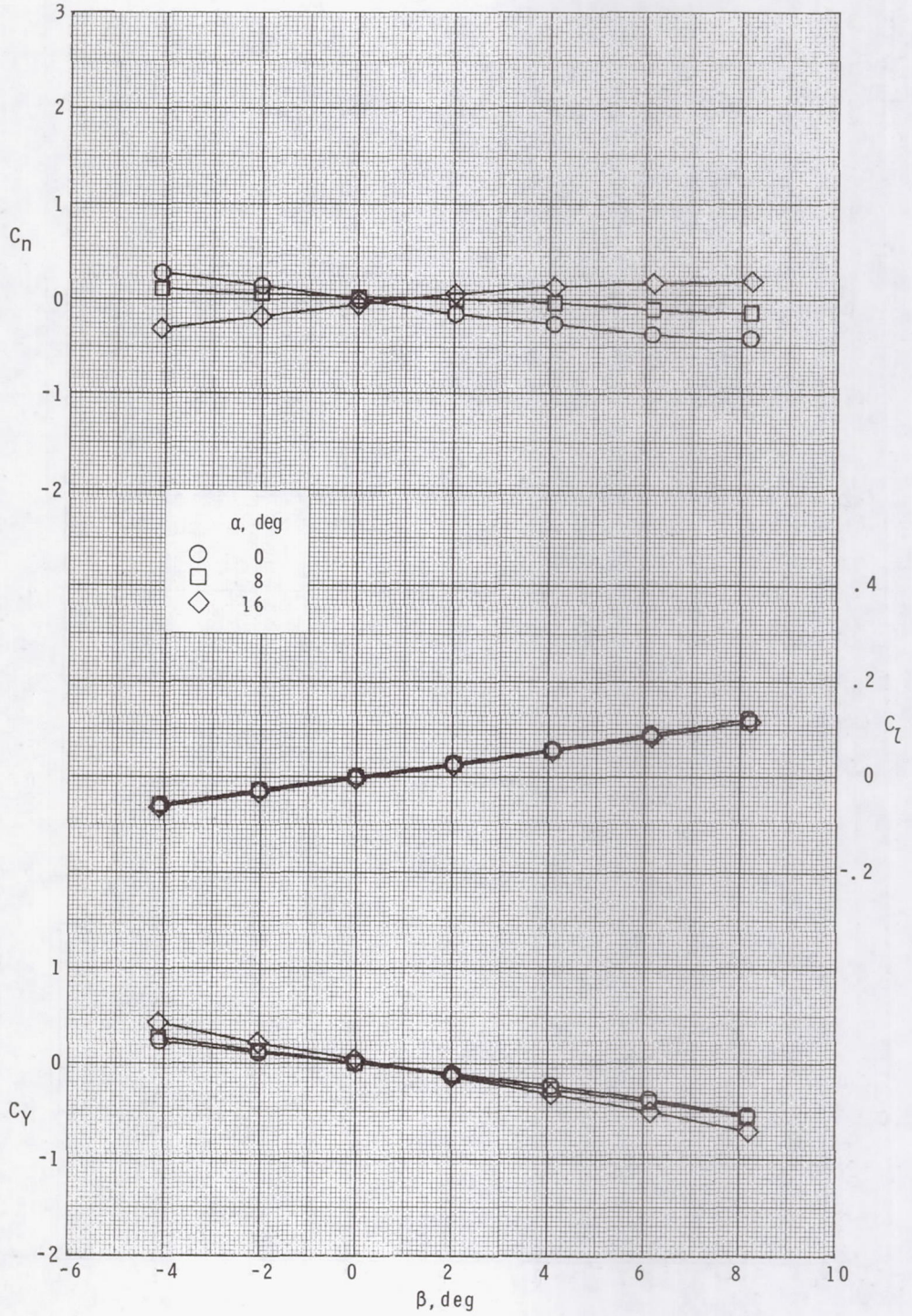

(c) Conf. 4; M = 1.47.

Figure 8.- Continued.

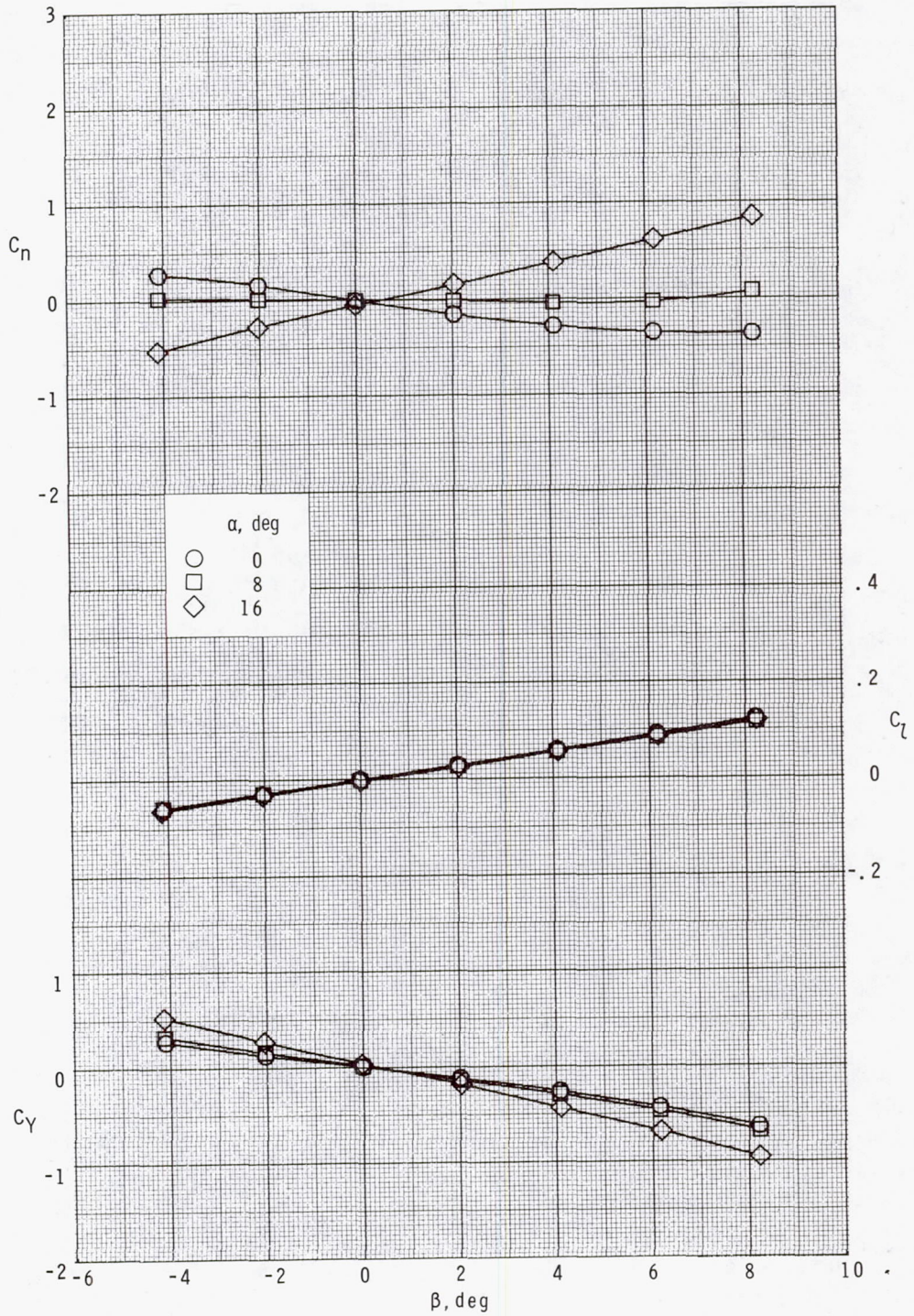

(d) Conf. 4; M = 2.16.

Figure 8.- Continued.

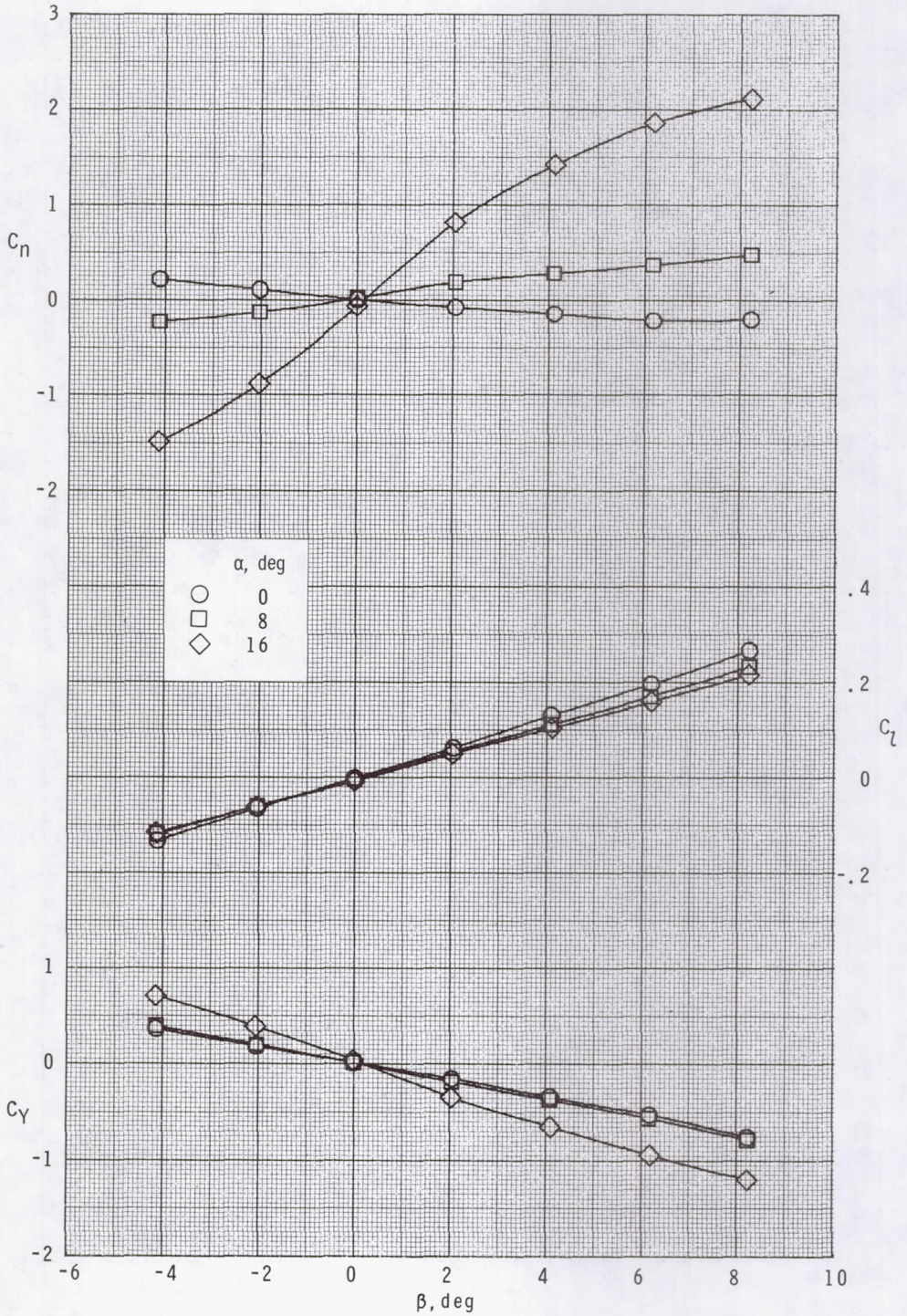

(e) Conf. 6; M = 1.47.

Figure 8.- Continued.

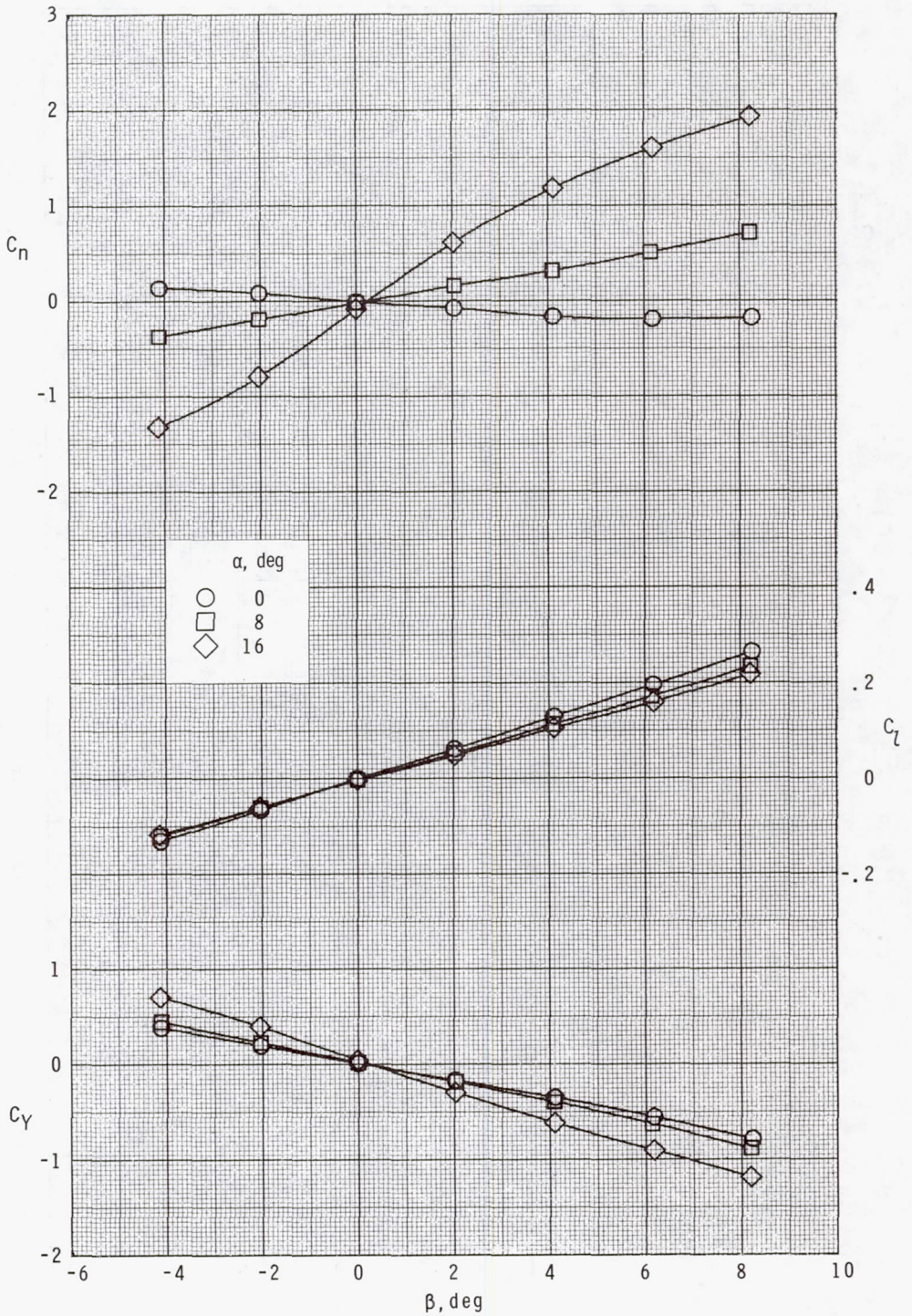

(f) Conf. 6; M = 2.16.

Figure 8.- Concluded.

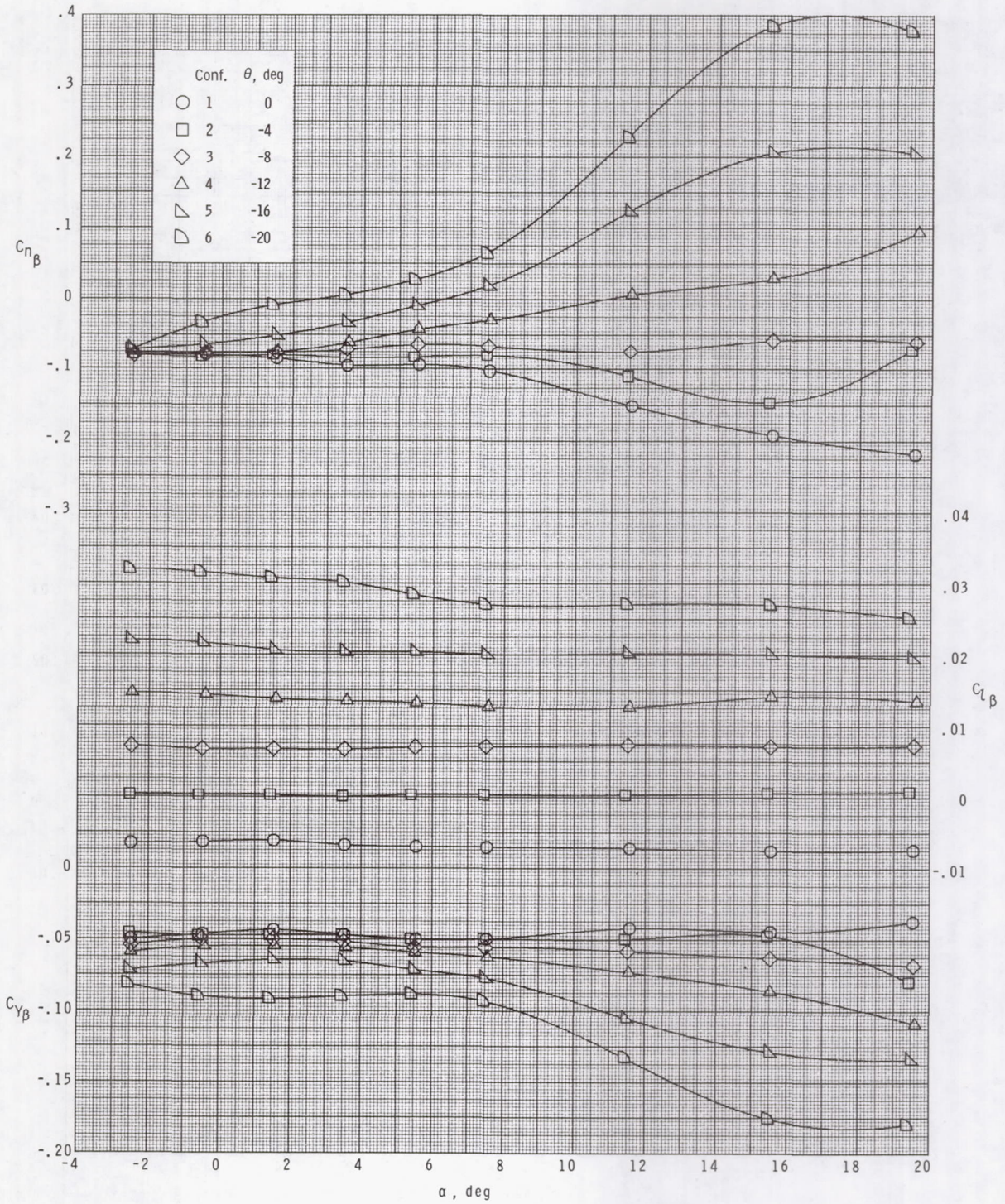

(a) M = 1.47.

Figure 9.- Variation of sideslip derivatives with angle of attack at supersonic speeds.

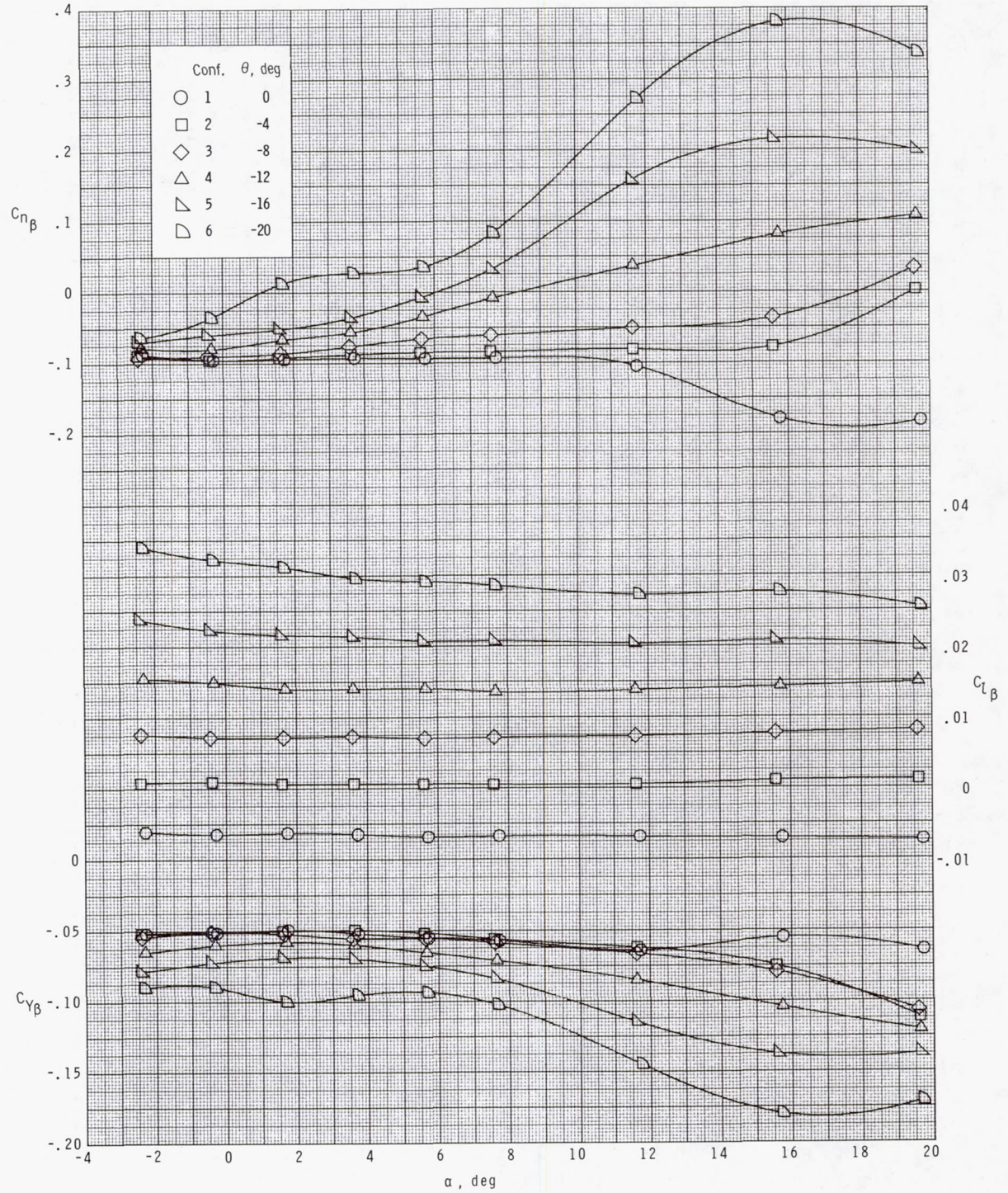

(b) M = 1.80.

Figure 9.- Continued.

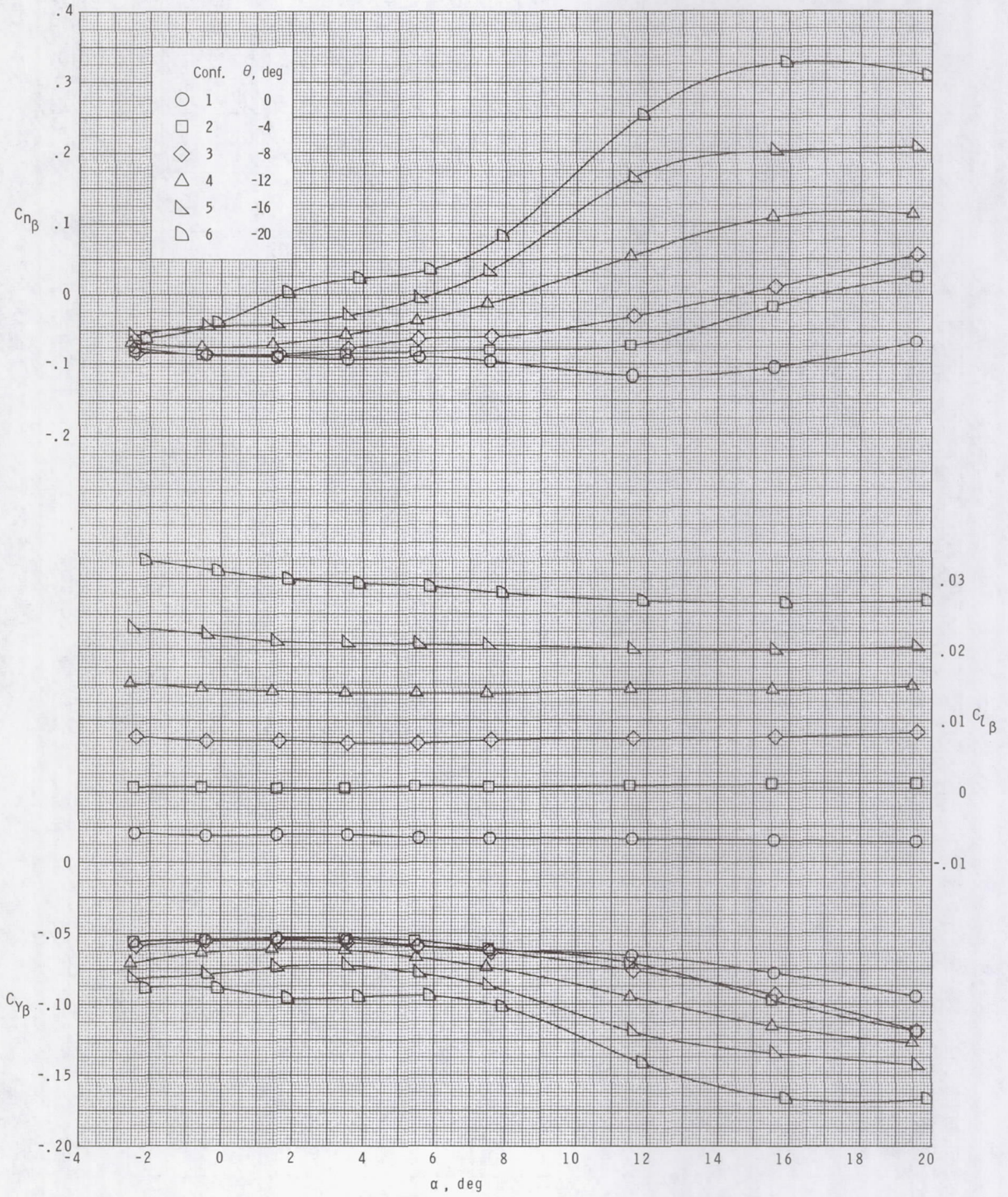

(c) M = 2.16.

Figure 9.- Concluded.

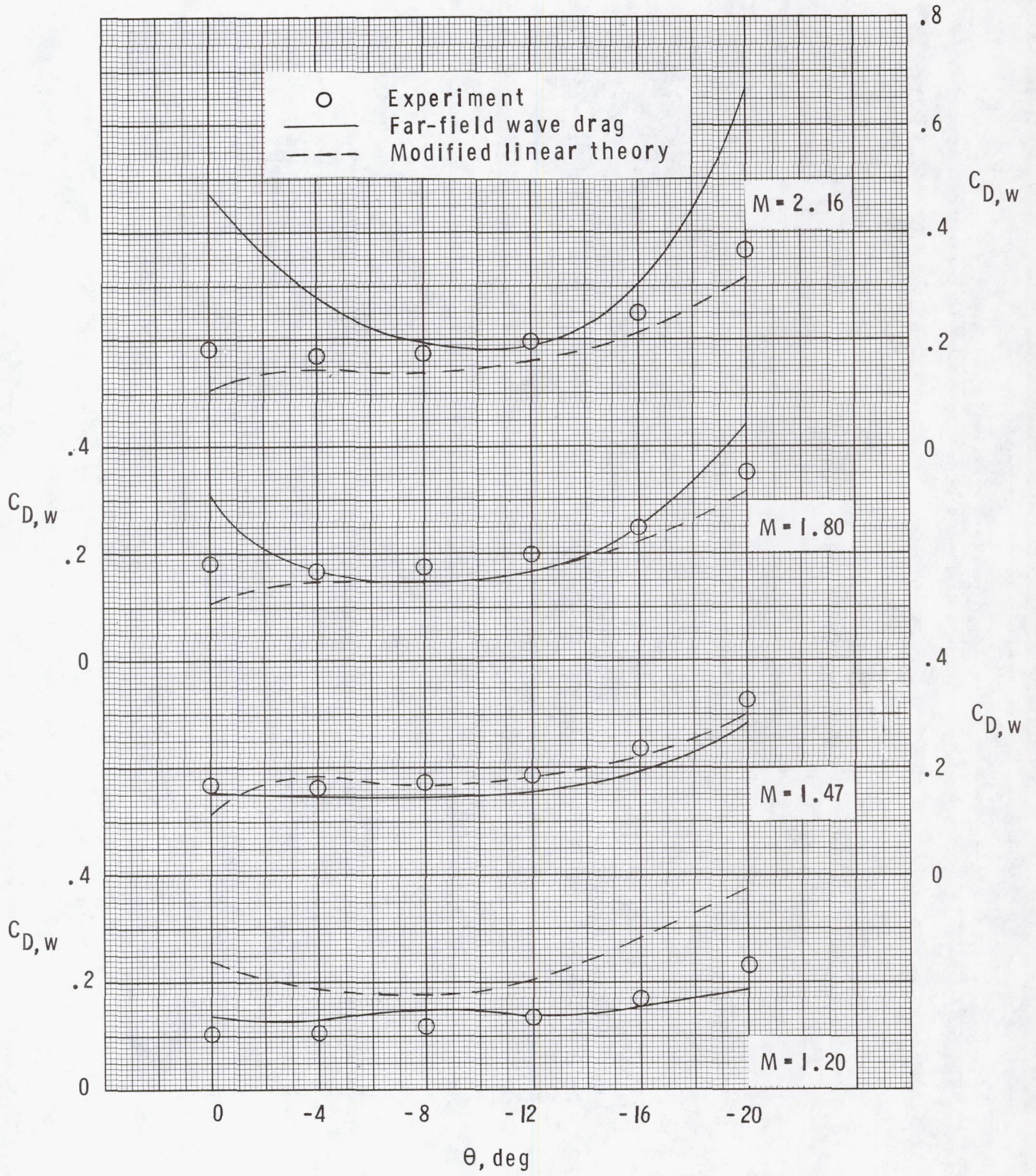

Figure 10.- Comparison of theory and experiment. $\alpha = 0°$.

1. Report No.	2. Government Accession No.	3. Recipient's Catalog No.
NASA TP-2206		

4. Title and Subtitle	5. Report Date
AERODYNAMIC CHARACTERISTICS OF A SERIES OF BODIES WITH VARIATIONS IN NOSE CAMBER	September 1983
	6. Performing Organization Code 505-43-23-10
7. Author(s) Barrett L. Shrout and Peter F. Covell	8. Performing Organization Report No. L-15647
	10. Work Unit No.
9. Performing Organization Name and Address NASA Langley Research Center Hampton, VA 23665	11. Contract or Grant No.
	13. Type of Report and Period Covered Technical Paper
12. Sponsoring Agency Name and Address National Aeronautics and Space Administration Washington, DC 20546	14. Sponsoring Agency Code

15. Supplementary Notes

16. Abstract

The aerodynamic characteristics of a series of cambered forebody models having a systematic variation in nose droop angle were determined from tests in the Langley 8-Foot Transonic Pressure Tunnel at Mach numbers from 0.60 to 1.20 and in the Langley Unitary Plan Wind Tunnel at Mach numbers of 1.47, 1.80, and 2.16. The models were tested through an angle-of-attack range of about 0° to 12° in the 8-Foot Transonic Pressure Tunnel and -2° to 20° in the Unitary Plan Wind Tunnel. Static longitudinal aerodynamic characteristics of the models were determined for all Mach numbers, and lateral-directional characteristics were determined for Mach numbers of 1.47 to 2.16. The investigation indicated that the principal effect of varying nose droop was on pitching moment, with some secondary effects on lift and drag. The experimental data were also compared with theoretical estimates.

17. Key Words (Suggested by Author(s))	18. Distribution Statement
Aerodynamic characteristics Wave drag Forebody Nose camber	Unclassified - Unlimited Subject Category 02

19. Security Classif. (of this report)	20. Security Classif. (of this page)	21. No. of Pages	22. Price
Unclassified	Unclassified	53	A04

For sale by the National Technical Information Service, Springfield, Virginia 22161

NASA-Langley, 1983